© 2015. Published by The Company of Biologists Ltd | Development (2015) 142, 2996-3008 doi:10.1242/dev.124586

RESEARCH ARTICLE

Kinesin-1 interacts with Bucky ball to form germ cells and is required to pattern the zebrafish body axis

Philip D. Campbell[1,*], Amanda E. Heim[1,*], Mordechai Z. Smith[1] and Florence L. Marlow[1,2,‡]

ABSTRACT

In animals, specification of the primordial germ cells (PGCs), the stem cells of the germ line, is required to transmit genetic information from one generation to the next. Bucky ball (Buc) is essential for germ plasm (GP) assembly in oocytes, and its overexpression results in excess PGCs in zebrafish embryos. However, the mechanistic basis for the excess PGCs in response to Buc overexpression, and whether endogenous Buc functions during embryogenesis, are unknown. Here, we show that endogenous Buc, like GP and overexpressed Buc-GFP, accumulates at embryonic cleavage furrows. Furthermore, we show that the maternally expressed zebrafish Kinesin-1 Kif5Ba is a binding partner of Buc and that maternal *kif5Ba* (M*kif5Ba*) plays an essential role in germline specification *in vivo*. Specifically, M*kif5Ba* is required to recruit GP to cleavage furrows and thereby specifies PGCs. Moreover, M*kif5Ba* is required to enrich Buc at cleavage furrows and for the ability of Buc to promote excess PGCs, providing mechanistic insight into how Buc functions to assemble embryonic GP. In addition, we show that M*kif5Ba* is also essential for dorsoventral (DV) patterning. Specifically, M*kif5Ba* promotes formation of the parallel vegetal microtubule array required to asymmetrically position dorsal determinants (DDs) towards the prospective dorsal side. Interestingly, whereas Syntabulin and *wnt8a* translocation depend on *kif5Ba*, *grip2a* translocation does not, providing evidence for two distinct mechanisms by which DDs might be asymmetrically distributed. These studies identify essential roles for maternal Kif5Ba in PGC specification and DV patterning, and provide mechanistic insight into Buc functions during early embryogenesis.

KEY WORDS: Bucky ball, Kinesin-1, Germ plasm, Dorsoventral patterning, Germ cell, Maternal

INTRODUCTION

In sexually reproducing animals, primordial germ cells (PGCs), germline stem cells that form the gametes, are specified early in development via induction by zygotic factors or inheritance of maternally deposited RNAs and proteins, termed germ plasm (GP) (Hartung and Marlow, 2014; Lesch and Page, 2012; Seervai and Wessel, 2013). Although key regulators of germline development are conserved, maternal inheritance modes utilize diverse regulators (e.g. *oskar* in insects and *buc* in vertebrates) and mechanisms of GP assembly (Hartung and Marlow, 2014; Lesch and Page, 2012; Seervai and Wessel, 2013). GP is both necessary and sufficient for germline specification (Hashimoto et al., 2004; Hathaway and Selman, 1961; Illmensee and Mahowald, 1974; Togashi et al., 1986), yet it remains mysterious how this process is regulated.

Maternal GP is produced in oocytes and assembled into ribonucleoprotein (RNP) complexes that are stabilized in specific subcellular locations (Hartung and Marlow, 2014). In zebrafish, maternal GP components, including *vasa*, *nanos3* and *dazl*, localize to the Balbiani body (Bb), an ancient asymmetric structure of primary oocytes (Howley and Ho, 2000; Kloc et al., 2004; Kosaka et al., 2007; Marlow, 2010). In zygotes, GP accumulates at distal cleavage furrows (Hashimoto et al., 2004; Knaut et al., 2000; Koprunner et al., 2001; Maegawa et al., 1999; Yoon et al., 1997), resulting in asymmetric inheritance of GP by four PGCs. After genome activation, GP is symmetrically inherited, resulting in four PGC clusters (Knaut et al., 2000). Although GP localization in zebrafish was first described nearly two decades ago, the molecular mechanisms governing GP inheritance remain elusive.

To date, zebrafish mutants disrupting GP assembly during early cleavages also perturb cleavages (Nair et al., 2013; Pelegri et al., 1999; Yabe et al., 2009). Both microtubule (MT) and F-actin networks are implicated in GP accumulation at cleavage furrows (Nair et al., 2013; Pelegri et al., 1999; Theusch et al., 2006; Yabe et al., 2009). MTs are enriched in distal cleavage furrows (Jesuthasan, 1998), and MT tips colocalize with GP-RNPs (Nair et al., 2013); however, it is unknown whether specific aggregation or stabilization factors exist and whether molecular motors are involved. Buc, a female germline-specific protein, is necessary and sufficient for Bb formation, in which GP localizes in primary oocytes (Bontems et al., 2009; Heim et al., 2014; Marlow and Mullins, 2008), and zebrafish and *Xenopus* Buc/Velo interact with RNAbps that bind GP-RNAs (Heim et al., 2014; Nijjar and Woodland, 2013). Furthermore, when *buc-gfp* RNA is injected into embryos, the translated Buc-GFP protein localizes to cleavage furrows, like GP, and increases PGC numbers (Bontems et al., 2009), indicating that exogenous Buc can promote PGC formation. Although maternal *buc* mutants do exist (Dosch et al., 2004; Marlow and Mullins, 2008), the polarity defects of *buc* oocytes preclude loss-of-function (LOF) analysis of potential Buc roles in GP recruitment in embryos.

In teleosts and amphibians, dorsoventral (DV) patterning, like germline specification, depends on maternally provided RNAs and proteins called dorsal determinants (DDs) (Langdon and Mullins, 2011; Marlow, 2010) that reside within the Bb and undergo Buc-dependent Bb-mediated translocation to the vegetal cortex (Ge et al., 2014; Lu et al., 2011; Nojima et al., 2010). Following fertilization, MT reorganization underlies dorsal determination (Houliston and Elinson, 1991; Jesuthasan and Strähle, 1997), as vegetal parallel microtubule arrays (pMTAs) govern asymmetric redistribution of the vegetally localized DDs relative to the animal-vegetal axis (Ge et al., 2014; Gerhart et al., 1989; Houliston and

[1]Department of Developmental and Molecular Biology, Albert Einstein College of Medicine, Yeshiva University, Bronx, NY 10461, USA. [2]Department of Neuroscience, Albert Einstein College of Medicine, Yeshiva University, Bronx, NY 10461, USA.
*These authors contributed equally to this work

‡Author for correspondence (florence.marlow@einstein.yu.edu)

Received 26 March 2015; Accepted 16 July 2015

Development (2015) 142, 2996-3008 doi:10.1242/dev.124586

Elinson, 1991; Jesuthasan and Strähle, 1997; Tran et al., 2012). In zebrafish, pMTA formation roughly coincides with asymmetric translocation of Syntabulin protein and *wnt8a* and *grip2a* RNAs (Ge et al., 2014; Lu et al., 2011; Nojima et al., 2010; Tran et al., 2012). Although maternal *grip2a* contributes to alignment and bundling of the pMTA (Ge et al., 2014), and vegetal MT plus-ends are oriented dorsalward (Tran et al., 2012), it remains unclear how pMTA rearrangements are initiated and which other factors are involved. Nevertheless, evidence from *Xenopus*, using antibodies and rigor mutants, implicates Kinesin-mediated transport of vegetal RNAs in oocytes (Gagnon et al., 2013; Messitt et al., 2008) and Kinesin-dependent pMTA formation (Marrari et al., 2000). Importantly, however, the specific Kinesin superfamily protein (Kif) involved is not known.

Here, we show that zebrafish maternal *kif5Ba* is essential for PGC specification and DV patterning. Our mutant analysis shows that maternal *kif5Ba* is dispensable for oocyte polarity, but acts in embryos to recruit GP to cleavage furrows, for PGC specification and for fertility. Moreover, Kif5Ba recruits or enriches Buc in cleavage furrows, where it probably mediates GP recruitment or stabilization, thus providing mechanistic insight into how GP is assembled at cleavage furrows. We further provide evidence for two mechanisms to asymmetrically distribute DDs in activated eggs: a *kif5Ba*-independent mechanism that mediates *grip2a* translocation, and a *kif5Ba*-dependent mechanism that organizes the pMTA and redistributes Syntabulin and *wnt8a*. These results provide mechanistic insight into Buc activities in embryos, PGC specification and the maternal mechanisms that generate DV asymmetry in early embryos.

RESULTS

Endogenous Buc localizes to the germ plasm of embryos and binds Kinesin-1

Buc is necessary and sufficient for GP recruitment in oocytes (Bontems et al., 2009; Heim et al., 2014; Marlow and Mullins, 2008), and, when overexpressed, Buc-GFP localizes to cleavage furrows in embryos (Bontems et al., 2009). However, it is unknown how Buc-GFP localizes to cleavage furrows and whether endogenous Buc does so, too. We examined endogenous Buc in cleavage-stage embryos using α-Buc antibodies (Heim et al., 2014) and found that endogenous Buc was enriched at distal cleavage furrows of wild-type (WT) embryos. These accumulations were cell cycle dependent, and were most apparent when chromosomes were decondensed (Fig. 1A; n=24/32 embryos with accumulation at ≥1 furrow) and rarely visible during mitosis (Fig. 1B; n=0/25 metaphase embryos and n=1/18 anaphase embryos). To investigate further Buc recruitment to cleavage furrows, we performed a pull-down assay from ovary lysates using anti-Buc antibody and identified Kif5B as a binding partner by mass spectrometry (peptide threshold=95%; n=10 peptides; 7% coverage). To validate this interaction, we performed co-immunoprecipitation assays in HEK293T cells using GFP-Buc and HA-tagged Kif5Ba. Immunoprecipitation with anti-GFP showed that GFP-Buc, but not GFP, co-precipitated HA-Kif5Ba (Fig. 1C). To determine whether Kif5Ba and Buc colocalize *in vivo* we injected exogenous *ha-kif5Ba* and *gfp-buc* RNA into WT eggs. At the 16-cell stage, GFP-Buc was enriched in cleavage furrows as previously reported (Bontems et al., 2009), whereas HA-Kif5Ba was uniformly distributed (Fig. 1D-F). Together with our previous studies showing that *kif5Ba* is the main maternally expressed *kif5* (Campbell and Marlow, 2013), these results indicate that Kif5Ba binds Buc and might mediate Buc localization in embryos.

kif5Ba recruits germ plasm RNAs to cleavage furrows and promotes germ cell specification

To test potential Kif5Ba involvement in localizing Buc, we generated zebrafish *kif5Ba* mutants using CRISPR-Cas9 mutagenesis (Chang et al., 2013; Hruscha et al., 2013) to disrupt the Kif5Ba motor domain (Fig. 1G). Two alleles were recovered and propagated. Sequencing of genomic DNA of F_1 progeny and cDNA of homozygous mutants identified a 5 base pair (bp) deletion predicted to produce a premature stop codon (*kif5Ba*^{ae11}) and a 6 bp deletion predicted to delete two amino acids (*kif5Ba*^{ae12}) (Fig. 1H). qRT-PCR revealed nonsense-mediated decay of *kif5Ba*^{ae11} but not of *kif5Ba*^{ae12} transcripts in homozygous mutants (Fig. 1I). Despite mild craniofacial defects of *kif5Ba*$^{ae12/ae12}$ but not of *kif5Ba*$^{ae11/ae11}$ mutant larvae (data not shown), fertile adult homozygotes and transheterozygotes were recovered; thus, zygotic *kif5Ba* is dispensable through adulthood.

We next assessed germ cell specification in maternal *kif5Ba* mutants, hereafter called M*kif5Ba* mutants, by examining GP-RNA localization in progeny of *kif5Ba*$^{-/-}$ females. During the first three cell cleavages, GP components accumulate at distal cleavage furrows and thereby become enriched in PGCs (Eno and Pelegri, 2013; Hashimoto et al., 2004; Knaut et al., 2000; Koprunner et al., 2001; Maegawa et al., 1999; Nair et al., 2013; Yabe et al., 2009; Yoon et al., 1997). The GP-RNAs *nanos3* and *vasa* accumulated at the cleavage furrows of 4-cell-stage embryos (Fig. 2A,E) and later in PGCs of shield stage WT (Fig. 2C,G), but not at the furrows of M*kif5Ba* embryos (Fig. 2B,F); and thus, no PGCs were detected in M*kif5Ba* mutants (Fig. 2D,H). Conversely, vegetal localization of *dazl* RNA was intact in M*kif5Ba* mutant embryos (Fig. 2I,J), suggesting that vegetal localization occurs independently of *kif5Ba*. Although GP-RNAs were absent from furrows, RT-PCR confirmed their presence in WT and M*kif5Ba* embryos through 2 h post-fertilization (hpf) (Fig. 2K), suggesting that *kif5Ba* mediates furrow enrichment.

PGCs reach gonad anlagen at 30 hpf (Raz and Reichman-Fried, 2006). In WT embryos, Vasa^{+} PGCs localized adjacent to the yolk extension (Fig. 2L,M), but were absent in M*kif5Ba* mutants (Fig. 2N,O), indicating failed PGC specification. Consequently, M*kif5Ba* embryos developed exclusively as sterile males (Table 1) devoid of germ cells (Fig. 2P-Q″). These results indicate that maternal *kif5Ba* is essential for GP recruitment to cleavage furrows, for PGC specification and for fertility.

Germ plasm RNA localization is intact in *kif5Ba* mutant oocytes

In primary oocytes, GP components are enriched in the Bb (Hartung and Marlow, 2014; Kosaka et al., 2007) in a Buc-dependent manner (Bontems et al., 2009; Heim et al., 2014; Marlow and Mullins, 2008). After Bb translocation to the vegetal pole, it disperses in stage-II oocytes; thereafter, GP component localization diverges (Hartung and Marlow, 2014; Braat et al., 1999; Knaut et al., 2000; Kosaka et al., 2007; Draper et al., 2007; Howley and Ho, 2000; Maegawa et al., 1999). RT-PCR analysis indicated that GP-RNAs were present in embryos; however, impaired GP-RNA localization in oocytes could cause GP defects in embryos. Buc protein localization and H&E staining, labeling with the ER and mitochondria marker DiOC6, confirmed that oocyte polarity was intact in *kif5Ba*$^{-/-}$ primary oocytes (supplementary material Fig. S1A,B,E-H). Later-stage oocytes also appeared grossly normal (supplementary material Fig. S1C,D). Fluorescent *in situ* hybridization (FISH) (Gross-Thebing et al., 2014) revealed enrichment of *vasa* and *nanos3* RNAs in the Bbs of WT and *kif5Ba*$^{-/-}$ mutants (supplementary

Development (2015) 142, 2996-3008 doi:10.1242/dev.124586

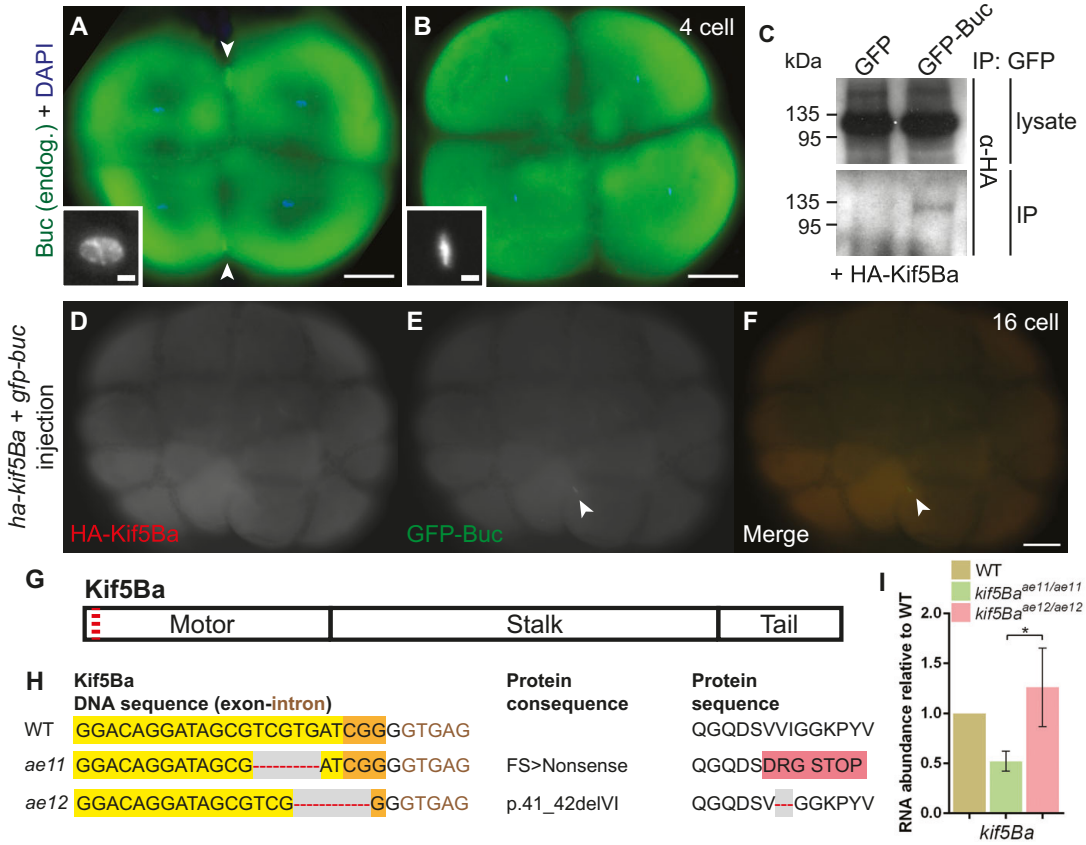

Fig. 1. Endogenous Buc localizes to the germ plasm of embryos and binds Kinesin-1. (A,B) Endogenous Buc localizes to distal cleavage furrows of 4-cell embryos when chromosomes are decondensed (A), but not during metaphase (B) or anaphase. Insets show DAPI. Arrowheads indicate Buc accumulation. Scale bars: 100 µm for main images, 10 µm for insets. See text for quantification. (C) GFP-Buc, but not GFP, co-immunoprecipitates HA-Kif5Ba in HEK293T cells. (D-F) Overexpressed GFP-Buc localizes to cleavage furrows and overexpressed HA-Kif5Ba is expressed throughout blastomeres, potentially allowing them to interact *in vivo*. Arrowheads indicate Buc accumulation. (G) Schematic protein structure of Kif5Ba, illustrating motor, stalk and tail domains. Red dashed line indicates CRISPR target site. (H) DNA and predicted protein sequences of WT and mutant *kif5Ba* alleles (*ae11 and ae12*). Yellow indicates protospacer, orange indicates PAM, gray area/red dashed line indicates a deletion and pink indicates altered amino acids. (I) qRT-PCR for *kif5Ba* from pools of 5-dpf WT and homozygous mutants. *kif5Ba* undergoes nonsense-mediated decay in *kif5Ba*$^{ae11/ae11}$ but not *kif5Ba*$^{ae12/ae12}$ mutants. Error bars show mean±s.e.m.; Student's *t*-test, **P*=0.0388.

material Fig. S1I-L,O-R). Moreover, *vasa* and *nanos3* were comparable in WT and *kif5Ba*$^{-/-}$ oocytes after Bb dispersal (supplementary material Fig. S1M,N,S,T). Together, these results show that *kif5Ba* is dispensable for animal-vegetal polarity and GP-RNA localization in oocytes, suggesting that maternal *kif5Ba* probably acts to recruit GP in embryos.

Cleavage furrows appear normal in M*kif5Ba* mutants

Several lines of evidence indicate that cleavage furrow integrity and cytoskeletal architecture are crucial for GP recruitment to furrows. First, maternal-effect mutants that disrupt cytokinesis disrupt GP aggregation (Nair et al., 2013; Pelegri et al., 1999; Yabe et al., 2009). Second, during cytokinesis the cleavage furrow is flanked by MTs oriented perpendicular to the furrow, known as the furrow microtubule array (FMA), (Jesuthasan, 1998). During furrow maturation, FMA enrichment resembles that of GP, and angles to form a distal furrow-oriented V-like structure. Finally, MT inhibitors disrupt the FMA and GP aggregation (Nair et al., 2013; Pelegri et al., 1999; Theusch et al., 2006). We investigated furrow-associated F-actin integrity in M*kif5Ba* embryos and found no differences between WT and M*kif5Ba* embryos in the medial contractile band, the F-actin accumulations flanking the FMA, nor in the circumferential actin bands around the blastomeres (supplementary material Fig. S2A-F) (Theusch et al., 2006; Urven et al., 2006). β-tubulin staining confirmed that FMA MTs properly formed adjacent to the F-actin contractile band, with an intervening MT-free zone (supplementary material Fig. S2C-F), and angled MTs distally (supplementary material Fig. S2G,H). These results indicated that failed GP recruitment in M*kif5Ba* embryos was not due to furrow-associated cytoskeleton abnormalities.

Providing exogenous *kif5Ba* to M*kif5Ba* mutants following fertilization rescues PGC specification

Because oocytes and cleavage furrows were intact, and GP components were available but not recruited in M*kif5Ba* embryos, we hypothesized that injection of *kif5Ba* RNA into M*kif5Ba* embryos might rescue GP recruitment and PGC specification. Unlike WT embryos, which recruited *nanos3* RNA to the first three cleavage furrows (Fig. 3A; *n*=22/24 embryos), enriched *nanos3* RNA in PGCs at sphere stage (Fig. 3D; 3.14±0.41 PGCs/embryo; *n*=28 embryos) and had clusters of Vasa^{+} PGCs at 30 hpf (Fig. 3G; 13.24±4.09 PGCs/side; *n*=21 embryos), M*kif5Ba* mutants failed to recruit *nanos3* to cleavage furrows (Fig. 3B; *n*=18/18 embryos) and thus lacked PGCs at sphere stage (Fig. 3E; 0.01±0.01 PGCs/embryo; one PGC in *n*=1/73, zero in *n*=72/73 embryos) and 30 hpf (Fig. 3H; zero PGCS in *n*=35/35 embryos). Injection of *ha-kif5Ba* RNA into M*kif5Ba* embryos, however,

Development (2015) 142, 2996-3008 doi:10.1242/dev.124586

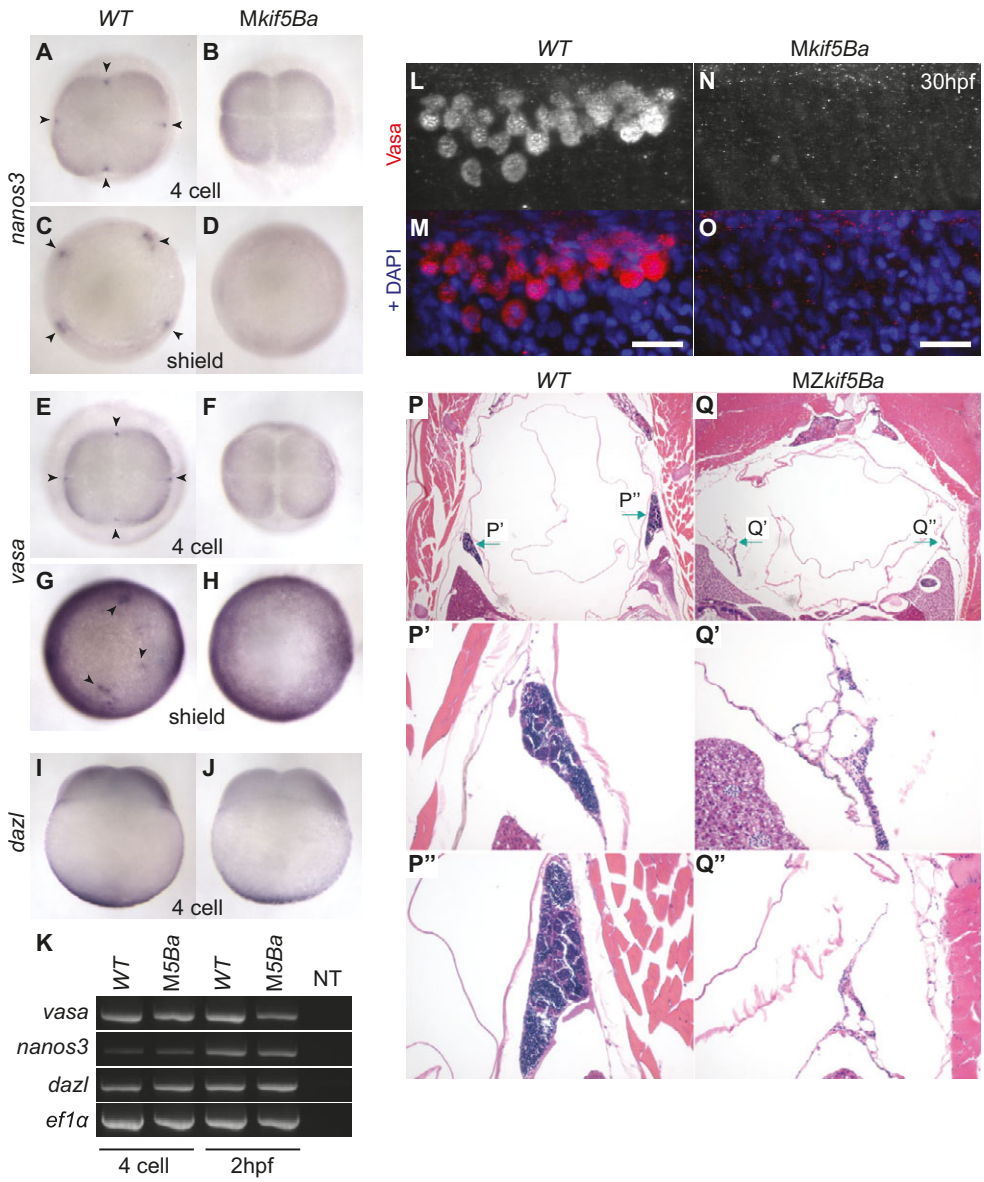

Fig. 2. *kif5Ba* recruits germ plasm RNAs to cleavage furrows and promotes germ cell specification. (A,B,E,F) *nanos3* (A,B) and *vasa* (E,F) localize to distal furrows in WT (A,E), but not in M*kif5Ba* mutants (B,F), at 4-cell stage. Arrowheads indicate *nanos3* and *vasa* accumulations. [*nanos3*: *n*=1/28 for M*kif5Ba*$^{ae11/ae12}$ (*N*=2 females), *n*=0/15 for M*kif5Ba*$^{ae11/ae11}$ (*N*=1 female), *n*=30/36 for WT (*N*=2 females) embryos have signal at ≥1 furrow; *vasa*: *n*=0/17 for M*kif5Ba*$^{ae11/ae12}$ (*N*=1 female), *n*=0/19 for M*kif5Ba*$^{ae11/ae11}$ (*N*=1 female), *n*=0/12 for M*kif5Ba*$^{ae12/ae12}$ (*N*=1 female), *n*=31/31 for WT (*N*=2 females) embryos have signal at ≥1 furrow.] (C,D,G,H) *nanos3* (C,D) and *vasa* (G,H) are enriched in PGCs in WT (C,G), but not in M*kif5Ba* mutants (D,H) at shield stage. Arrowheads indicate PGCs. [*nanos3*: *n*=0/32 for M*kif5Ba*$^{ae11/ae12}$ (*N*=2 females), *n*=0/19 for M*kif5Ba*$^{e1/e1}$ (*N*=1 female), *n*=28/28 for WT (*N*=2 females) embryos have PGCs; *vasa*: *n*=0/18 for M*kif5Ba*$^{ae11/ae12}$ (*N*=1 female), *n*=0/22 for M*kif5Ba*$^{ae11/ae11}$ (*N*=1 female), *n*=0/17 for M*kif5Ba*$^{ae12/ae12}$ (*N*=1 female), *n*=37/37 for WT (*N*=2 females) embryos have PGCs.] (I,J) Vegetal localization of *dazl* is intact in WT (I) and M*kif5Ba* mutants (J) at 4-cell stage. [*n*=19/19 for M*kif5Ba*$^{ae11/ae12}$ (*N*=2 females), *n*=20/20 for WT (*N*=2 females) embryos have vegetal signal.] (K) RT-PCR shows that germ plasm RNAs *vasa*, *nanos3* and *dazl* are inherited by WT and M*kif5Ba* mutant eggs (4-cell stage) and are maintained in WT and M*kif5Ba* embryos (2 hpf). *ef1α*, loading control. NT, no template. (L-O) Vasa^{+} PGCs are present in WT (L,M) but not in M*kif5Ba* mutant (N,O) embryos at 30 hpf. Scale bars: 10 µm. [*n*=0/48 for M*kif5Ba*$^{ae11/ae12}$ (*N*=2 females), *n*=19/67 for M*kif5Ba*$^{ae11/ae11}$ (*N*=3 females), *n*=0/20 for M*kif5Ba*$^{ae12/ae12}$ (*N*=3 females), *n*=53/53 for WT (*N*=4 females) have PGCs.] (P-Q″) H&E-stained transverse sections of adult WT (P) and MZ*kif5Ba* mutants (Q) show that MZ*kif5Ba* testes (green arrows) lack germ cells. P′,Q′ and P″,Q″ are higher magnification images of left and right testes, respectively. [*n*=4/4 M*kif5Ba*$^{ae12/ae12}$ adult males had empty testes; in addition, *n*=18/18 adult M*kif5Ba*$^{ae11/ae12}$ males dissected had testes devoid of germ cells.]

promoted *nanos3* RNA recruitment to one or two furrows (Fig. 3C; *n*=6/32 embryos), and a small number of PGCs were detected at sphere stage (Fig. 3F; 0.15±0.04 PGCs/embryo; one PGC in *n*=13/85, zero in *n*=72/85 embryos) and 30 hpf (Fig. 3I; *n*=6/45 embryos with PGCs; 2.00±1.10 PGCs/side in those embryos with PGCs). Importantly, injection of RNA encoding Cherry had no effect on PGC number in WT nor did it rescue PGC number in M*kif5Ba* mutants (supplementary material Fig. S3). Together, these results suggest that Kif5Ba functions after fertilization to mediate GP recruitment to the cleavage furrows.

Kif5Ba localizes Buc to cleavage furrows and mediates germ plasm assembly in embryos

Because *kif5Ba* RNA injection restored GP recruitment in M*kif5Ba* mutants, we postulated that Kif5Ba localizes a GP recruitment or aggregation factor. Based on its localization to cleavage furrows

Development (2015) 142, 2996-3008 doi:10.1242/dev.124586

Table 1. M*kif5Ba* and MZ*kif5Ba* adult mutants are sterile males

Genotype	Maternal genotype	Paternal genotype	Phenotypically male progeny	Egg fertilization assay
kif5Ba$^{ae11/ae11}$	*kif5Ba*$^{ae11/ae11}$	*kif5Ba*$^{ae11/ae11}$	100% (*n*=8)	100% unfertilized (*N*=4 adults screened, *n*=360 eggs total)
kif5Ba$^{ae11/ae11}$, *kif5Ba*$^{ae11/ae12}$ or *kif5Ba*$^{e12/e12}$	*kif5Ba*$^{ae11/ae12}$	*kif5Ba*$^{ae11/ae12}$	100% (*n*=23)	100% unfertilized (*N*=9 adults screened, *n*=1218 eggs total)
kif5Ba$^{ae12/ae12}$	*kif5Ba*$^{ae12/ae12}$	*kif5Ba*$^{ae12/ae12}$	100% (*n*=10)	100% unfertilized (*N*=6 adults screened, *n*=395 eggs total)
kif5Ba$^{ae12/+}$	*kif5Ba*$^{ae12/ae12}$	*kif5Ba*$^{ae12/+}$	100% (*n*=10)	100% unfertilized (*N*=3 adults screened, *n*=203 eggs total)

(Fig. 1), its ability to promote excess PGCs when overexpressed (Bontems et al., 2009), and its interaction and colocalization with Kif5Ba (Fig. 1), we hypothesized that Kif5Ba might mediate GP recruitment or stabilization by localizing Buc. Therefore, we injected GFP-Buc into 1-cell-stage WT or M*kif5Ba* mutant embryos and examined its localization. GFP-Buc accumulated at distal cleavage furrows of WT embryos (*n*=32/32), as previously reported (Bontems et al., 2009), but was not recruited in most M*kif5Ba* mutants (Fig. 4A,B; *n*=45/62). When present at the furrows of mutants, GFP-Buc did not aggregate distally but remained distributed along the furrow (*n*=17/62). Like GFP-Buc, endogenous Buc was enriched at distal furrows of WT (*n*=24/32 have Buc at ≥1 furrow), but this rarely occurred in M*kif5Ba* mutants (*n*=4/32 have Buc at ≥1 furrow) (Fig. 4C,D). Together with our binding data, these results suggest that Kif5Ba enriches Buc and GP at cleavage furrows.

Next, we tested whether Kif5Ba was required to increase PGC numbers in embryos overexpressing Buc. As previously reported (Bontems et al., 2009), additional *nanos3*$^{+}$ cells were detected in GFP-Buc-injected WT compared with uninjected siblings at 4 hpf (Fig. 4E,F; *n*=10 uninjected and injected embryos with averages of 4.0 and 5.7 cells, respectively; *P*=0.0314, Student's *t*-test:). By contrast, GFP-Buc produced no increase in *nanos3*$^{+}$ cells in M*kif5Ba* mutants (Fig. 4G,H; *n*=3/63 uninjected and 6/50 injected: averages of 0.05 and 0.14 PGCs, respectively; *P*=0.1221, Student's *t*-test). These results indicate that Kif5Ba is required to promote excess PGC formation in response to Buc overexpression and that the presence of Buc at the cleavage furrows is integral to GP assembly.

Maternal *kif5Ba* is required for proper dorsoventral patterning

In addition to lacking germ cells, M*kif5Ba* mutants were ventralized to varying degrees at 1 day post-fertilization (dpf) (Fig. 5A-F), ranging from lack of notochord (V1, Fig. 5B) to complete axis radialization (V5, Fig. 5F). Additionally, a subset had secondary axes with duplicated rostral structures and a fused caudal body (Fig. 5G,G′), reminiscent of M*grip2a* mutants (Ge et al., 2014). Because ventralization was only observed in progeny of homozygous *kif5Ba*$^{ae11/ae11}$ and *kif5Ba*$^{ae12/ae12}$ and transheterozygous *kif5Ba*$^{ae11/ae12}$ females, but not WT or heterozygous genotypes, we concluded that *kif5Ba* mutation caused ventralization (Fig. 5H). *kif5Ba*$^{ae11/ae12}$ and *kif5Ba*$^{ae12/ae12}$ were more severe than *kif5Ba*$^{ae11/ae11}$ females, and had similar penetrance and expressivity. No phenotypes were observed in

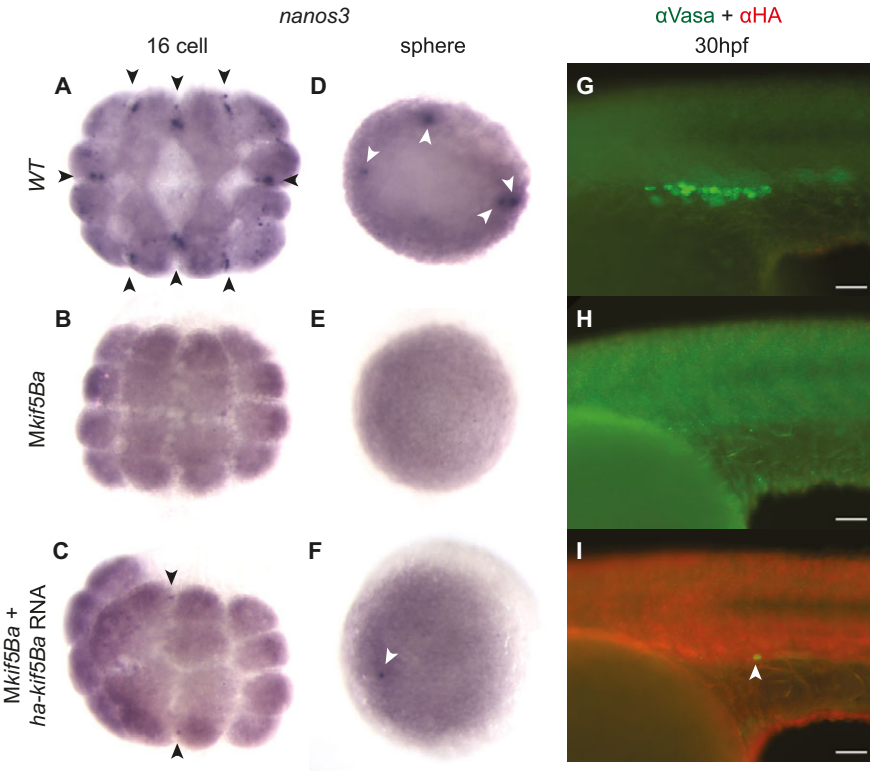

Fig. 3. Overexpression of *kif5Ba* in M*kif5Ba* mutants following fertilization is sufficient to specify germ cells. (A-C) *nanos3* RNA is recruited to the first three cleavage furrows in WT (A) but is not recruited to furrows in M*kif5Ba* mutants (B) at 16-cell stage. Injection of *ha-kif5Ba* restores *nanos3* recruitment to 1-2 furrows in a fraction of M*kif5Ba* mutants (C). Black arrowheads denote recruited *nanos3*. (D-F) *nanos3* RNA becomes enriched in the prospective PGCs of WT (D) but is not enriched in M*kif5Ba* mutants (E). Injection of *ha-kif5Ba* restores *nanos3* enrichment to one PGC in a fraction of M*kif5Ba* mutants (F). White arrowheads denote PGCs. (G-I) Vasa^{+} PGCs are present in WT (G) but not in M*kif5Ba* mutants (H) at the yolk-yolk extension intersection. Injection of *ha-kif5Ba* restores small numbers of PGCs in M*kif5Ba* mutants (arrowhead in I). See text for quantification. Scale bars: 50 µm.

Development (2015) 142, 2996-3008 doi:10.1242/dev.124586

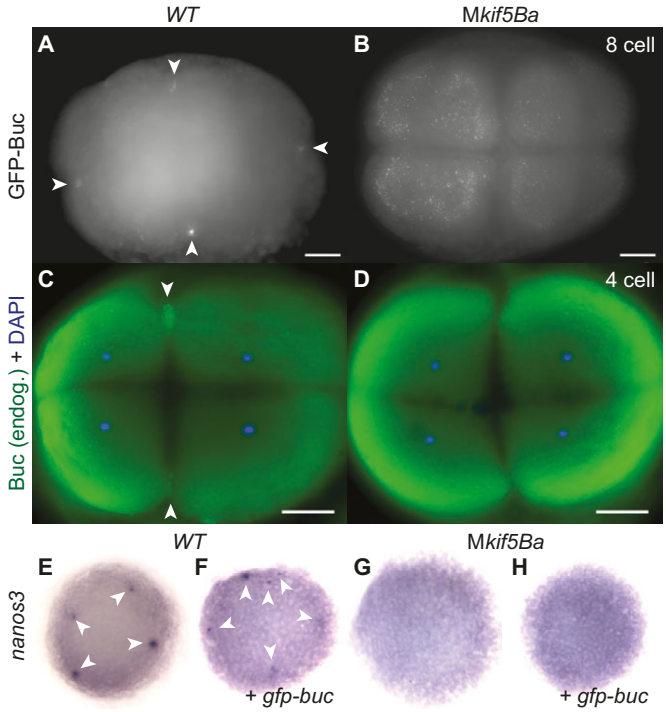

Fig. 4. Kif5Ba localizes Buc to cleavage furrows to mediate germ plasm assembly in the embryo. (A,B) GFP-Buc is recruited to distal furrows of WT (arrowheads in A) but not of M*kif5Ba* mutants (B). [*n*=0/29 for M*kif5Ba*$^{ae11/ae12}$ (*N*=2 females), *n*=0/18 for M*kif5Ba*$^{ae11/ae11}$ (*N*=3 females), *n*=0/15 for *kif5Ba*$^{ae12/ae12}$ (*N*=1 female), *n*=32/32 for WT (*N*=4 females) have compact distal GFP-Buc; *n*=2/29 for M*kif5Ba*$^{ae11/ae12}$, *n*=15/18 for M*kif5Ba*$^{ae11/ae11}$, *n*=0/15 for M*kif5Ba*$^{ae12/ae12}$ have some furrow recruitment of GFP-Buc, although distal furrow compaction is defective.] (C,D) Endogenous Buc localizes to distal cleavage furrows of WT (arrowheads in C) but not M*kif5Ba* mutants (D). [*n*=2/15 for M*kif5Ba*$^{ae12/ae12}$ (*N*=2 females), *n*=2/17 for M*kif5Ba*$^{ae11/ae11}$ (*N*=1 female), *n*=24/32 for WT (*N*=4 females) of cells with decondensed chromosomes have Buc at ≥1 distal cleavage furrow.] (E-H) Compared with uninjected WT (E), *gfp-buc* injected WT (F) embryos have additional *nanos3*$^{+}$ PGCs (arrowheads), whereas uninjected (G) and *gfp-buc*-injected (H) M*kif5Ba* mutants lacked *nanos3*$^{+}$ cells. See text for quantification.

heterozygotes for either allele. Together, these results are consistent with both *kif5Ba*^{ae11} and *kif5Ba*^{ae12} having LOF character, with *kif5Ba*^{ae12} probably being a stronger LOF allele than *kif5Ba*^{ae11}. Although unlikely, we cannot exclude the possibility that *kif5Ba*^{ae12} acts as a weak dominant negative allele by dimerizing with other Kifs to form non-functional motors or competing for cargo.

kif5Ba localizes dorsal determinants in the activated egg

Dorsal specification in zebrafish is apparent around the mid-blastula transition and can be detected by nuclear β-catenin accumulation in dorsal blastomeres (Schneider et al., 1996), although *syntabulin* (*sybu*) and *grip2a* maternal mutants show that DV patterning begins earlier (Ge et al., 2014; Nojima et al., 2010). These maternal factors are thought to mediate dorsalward translocation of vegetally localized factors, including *wnt8a* RNA, during the first hour following fertilization. Asymmetry in *wnt8a* RNA is postulated to translate into asymmetric Wnt8a protein distribution and eventually β-catenin activation in dorsal blastomeres (Lu et al., 2011).

To determine whether maternal Kif5Ba localizes maternal regulators of DV patterning, we performed *in situ* hybridization for *sybu*, *grip2a* and *wnt8a* RNA in eggs. As previously reported (Ge et al., 2014; Lu et al., 2011; Nojima et al., 2010), *sybu*, *grip2a* and *wnt8a* RNA were vegetally localized at 2 min post-egg activation (mpa) (Fig. 6A,F,J), and by 45 mpa *grip2a* and *wnt8a* RNA, but not *sybu* RNA, asymmetrically translocated in WT (Fig. 6C,H,L). In M*kif5Ba* mutants, *sybu* RNA was initially vegetally localized (Fig. 6B), but was more dispersed [*sybu* domain angle in M*kif5Ba* (*n*=57 eggs; 3 females) was 1.14-fold that of WT (*n*=57 eggs; 4 females); Student's *t*-test: $P=6.78\times10^{-8}$]. At 45 mpa, two *sybu* RNA expression classes, strong and weak, were observed in both WT and M*kif5Ba* mutants, although more M*kif5Ba* mutants showed weak expression (Fig. 6C-D′). qRT-PCR for *sybu* RNA confirmed that it was significantly elevated in M*kif5Ba* mutants at 2 mpa, and, although not significantly different, trended towards lower levels at 45 mpa (Fig. 6E). As no transcription occurs during this period, these results indicate that *sybu* RNA is not properly maintained in M*kif5Ba* mutants. Unlike *sybu* RNA, in M*kif5Ba* activated eggs *grip2a* and *wnt8a* RNA localization resembled WT initially (Fig. 6G,K; *grip2a* RNA mutant angle was 0.98±0.03 times that of WT and *wnt8a* RNA mutant angle was 1.07±0.05 times that of WT; Student's *t*-test, *P*=0.77 and *P*=0.43, respectively); however, by 45 mpa, *grip2a* translocated asymmetrically in M*kif5Ba* activated eggs (Fig. 6I,N), but *wnt8a* did not (Fig. 6M,N). These data suggest that *kif5Ba* maintains *sybu* RNA at the vegetal pole and is necessary for *wnt8a*, but not *grip2a*, RNA translocation.

Previous studies have shown that, like *grip2a* and *wnt8a* RNA, Syntabulin (Sybu) protein translocates after egg activation (Fig. 6O,P) (Nojima et al., 2010). In M*kif5Ba* activated eggs, Sybu protein, like *sybu* RNA, was mislocalized in some M*kif5Ba* eggs at 2 mpa, either aberrantly present on the lateral cortex or diffuse about the cortex (Fig. 6Q-Q″; Sybu was vegetally localized in *n*=3/12 M*kif5Ba*$^{ae11/ae12}$, *n*=4/9 M*kif5Ba*$^{ae11/ae11}$ and *n*=2/9 M*kif5Ba*$^{ae12/ae12}$ compared with *n*=13/15 WT eggs). At 45 mpa, in a subset of eggs, Sybu either failed to translocate or was not detectable (Fig. 6R-R″; Sybu translocated normally in *n*=1/11 M*kif5Ba*$^{ae11/ae12}$, *n*=12/18 M*kif5Ba*$^{ae11/ae11}$ and *n*=3/11 for M*kif5Ba*$^{ae12/ae12}$ compared with *n*=16/19 WT eggs). Thus, *kif5Ba* might function to maintain vegetal localization of Sybu and for its subsequent asymmetric movement. Because Sybu can link Kif5s and their cargo in other biological contexts (Cai et al., 2005; Su et al., 2004), and zebrafish Sybu and Kif5Ba interact *in vitro* (Nojima et al., 2010), Sybu probably localizes in oocytes or early embryos via its interaction with Kif5Ba.

To determine when Kif5Ba acts in DV patterning, we attempted to rescue the M*kif5Ba* ventralization phenotype by injecting *ha-kif5Ba* RNA into M*kif5Ba* embryos; however, this did not suppress the penetrance or expressivity of M*kif5Ba* ventralized phenotypes (Fig. 6S). Notably, other maternal-effect mutants that disrupt early translocation events also cannot be rescued by RNA injection after fertilization (Ge et al., 2014; Nojima et al., 2010). Together, these results are consistent with roles for Kif5Ba in positioning Sybu in oocytes or during egg activation.

Vegetal microtubules fail to organize in *kif5Ba* mutants

Prior to asymmetric translocation of Sybu protein and *wnt8a* RNA (~20 mpa), the vegetal MT network reorganizes to form the vegetal pMTA (Jesuthasan and Strähle, 1997), which predicts the DV axis (Tran et al., 2012). Disrupting this network, as occurs in M*grip2a* mutants (Ge et al., 2014), or by treating activated eggs with MT inhibitors, cold temperature or UV irradiation (Lu et al., 2011; Nojima et al., 2010), blocks Sybu protein and *wnt8a* RNA translocation. To determine whether M*kif5Ba* DV patterning defects were due to pMTA defects we analyzed the MT network of

Development (2015) 142, 2996-3008 doi:10.1242/dev.124586

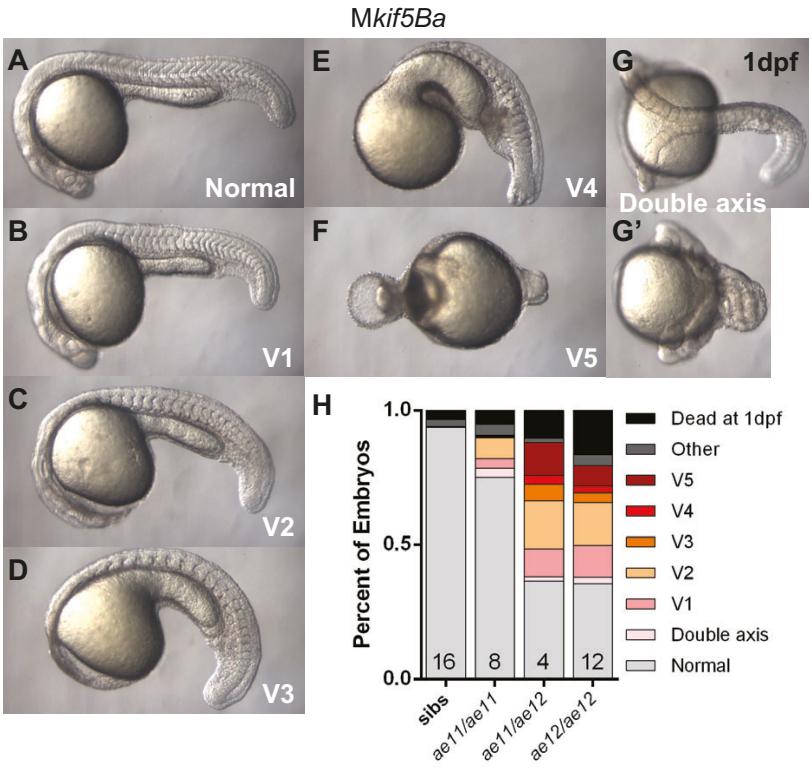

Fig. 5. Maternal *kif5Ba* is required for dorsal fate. (A-G) M*kif5Ba* mutant embryos are variably ventralized at 1 dpf: V1, nearly complete AP axis lacking notochord and blocky somites (B); V2, reduced head structures (C); V3, largely lacking head structures except the posteriormost ones (D); V4, lack all head structures but possess an AP axis (E); V5, completely radialized axis (F). A small fraction of mutant embryos had duplicated anterior axes with fused caudal bodies (G,G′). (H) Distribution of phenotypic classes for homozygous and transheterozygous M*kif5Ba* mutant embryos. The number of females assayed is indicated at the base of each bar. At least two clutches of embryos from each female were analyzed. Total number of embryos assayed for each genotype: *n*=1247 for M*kif5Ba*$^{ae11/ae12}$, *n*=2748 for M*kif5Ba*$^{ae11/ae11}$, *n*=2158 for M*kif5Ba*$^{ae12/ae12}$ and *n*=988 for siblings.

activated eggs. Surprisingly, although pMTA formation was robust in WT (Fig. 7A,M), it failed in most M*kif5Ba* activated eggs (Fig. 7D, M). Instead, M*kif5Ba* vegetal MTs either appeared bundled and randomly oriented (Fig. 7G,M) or non-bundled with a crosshatch appearance (Fig. 7J,M). No differences were observed between the lateral cortex MT networks of WT and M*kif5Ba* eggs (Fig. 7N,Q).

Cortical granules (CGs) are normally rapidly exocytosed following egg activation (Becker and Hart, 1999). Persisting CGs in zebrafish maternal-effect mutants disrupting *heterogeneous nuclear ribonucleoprotein I* (*hnRNPI*) are thought to interfere with vegetal pMTA formation and disrupt DV patterning (Mei et al., 2009). To determine whether persisting CGs could explain the disrupted pMTA in M*kif5Ba* mutants, CGs were labeled with *Maclura pomifera* agglutinin (MPA) lectin (Becker and Hart, 1996, 1999). M*kif5Ba* activated eggs at 25 mpa displayed variable CG exocytosis impairment (Fig. 7E,H,K); however, quantification of the number of retained CGs within a defined vegetal region revealed no difference in the density of CGs retained between M*kif5Ba* mutants, regardless of pMTA defect severity (Fig. 7M). Specifically, M*kif5Ba* mutants with severe CG exocytosis deficits but normal vegetal pMTAs and M*kif5Ba* mutants with mild CG exocytosis defects but disorganized MTs were observed (Fig. 7M). Furthermore, consistent with their more severe ventralization phenotypes, pMTA defects were more severe in M*kif5Ba*$^{ae12/ae12}$ mutants than M*kif5Ba*$^{ae11/ae11}$ mutants; however, the number of retained CGs was not significantly different between these genotypes (supplementary material Fig. S4A,B). Together, these data indicate that maternal *kif5Ba* mediates pMTA formation and CG exocytosis, but persisting CGs do not account for the cytoskeletal defects.

DISCUSSION

Our study identifies the key maternal motor required for specification of the germline and the DV axis in zebrafish (Fig. 8). Moreover, our findings that Kif5Ba binds to Buc, mediates Buc recruitment to the cleavage furrow, where GP assembles in the embryo, and is required for excess PGC formation in response to Buc overexpression, provide new insight into the mechanism by which Buc promotes germ plasm assembly in embryos. Furthermore, our studies show that Kif5Ba-mediated MT reorganization underlies cortical rotation-like events to promote asymmetric localization of Syntabulin and *wnt8a*, and that asymmetry of *grip2a* occurs independently of *kif5Ba*. Thus, our results provide evidence for distinct MT-dependent translocation events that mediate maternal DV patterning.

A Kif5Ba-Buc interaction required for germ plasm assembly and germline specification

Although germline development in all animals relies on conserved genetic factors, two main modes of germline specification exist (Ewen-Campen et al., 2010; Lesch and Page, 2012; Seervai and Wessel, 2013). Germline stem cells are either induced by zygotic factors or rely on the inheritance of maternal GP to specify PGCs (Dosch, 2014; Hartung and Marlow, 2014; Marlow, 2010). In zebrafish, GP-RNAs and proteins localize to the Bb of primary oocytes in a Buc-dependent manner (Bontems et al., 2009; Heim et al., 2014; Kosaka et al., 2007; Marlow and Mullins, 2008) and are later inherited and stabilized in the distal cleavage furrows during the first embryonic cleavage cycles (Hashimoto et al., 2004; Knaut et al., 2000; Koprunner et al., 2001; Maegawa et al., 1999; Theusch et al., 2006; Yoon et al., 1997). Manual ablation of GP prevents PGC specification (Hashimoto et al., 2004), indicating that it is essential for fertility; however, the mechanisms governing embryonic GP segregation are poorly understood.

Along with the absence of overt defects in oocyte polarity and GP localization in *kif5Ba* mutant ovaries, our *ha-kif5Ba* RNA injection rescue experiments provide compelling evidence that Kif5Ba functions during cleavage stages to localize GP components. However, RNA injection only partially suppresses deficits. Because

Development (2015) 142, 2996-3008 doi:10.1242/dev.124586

GP recruitment to the furrows only occurs between the 2-cell stage and 16-cell stage, the rescue activity of *ha-kif5Ba* RNA is probably limited by the time required to produce sufficient functional Kif5Ba protein during this 1.5-h window. Nonetheless, it is clear that exogenous *kif5Ba* RNA provided following fertilization can promote GP recruitment to cleavage furrows of 16-cell embryos, suggesting that endogenous Kif5Ba performs this function during the first three cleavages. Significantly, this is the first maternal factor identified in zebrafish that is required for GP recruitment which does not interfere with the furrow-associated cytoskeleton or cleavage furrow formation.

We have shown that endogenous Buc, a necessary factor for GP assembly in oocytes, localizes, like GP, to distal cleavage furrows of embryos. Furthermore, loss of Buc localization to furrows, as occurs in M*kif5Ba* mutants, coincides with failed GP recruitment and ultimately failure to specify PGCs. Additionally, although Buc overexpression can promote PGC formation in WT (Bontems et al., 2009), we show that this activity requires MKif5Ba; therefore, Buc probably acts at the furrow to recruit or stabilize GP. Because Buc interacts with RNAbps (Heim et al., 2014), it might recruit GP-RNPs indirectly, although we cannot exclude the possibility that Buc possesses uncharacterized RNA binding elements.

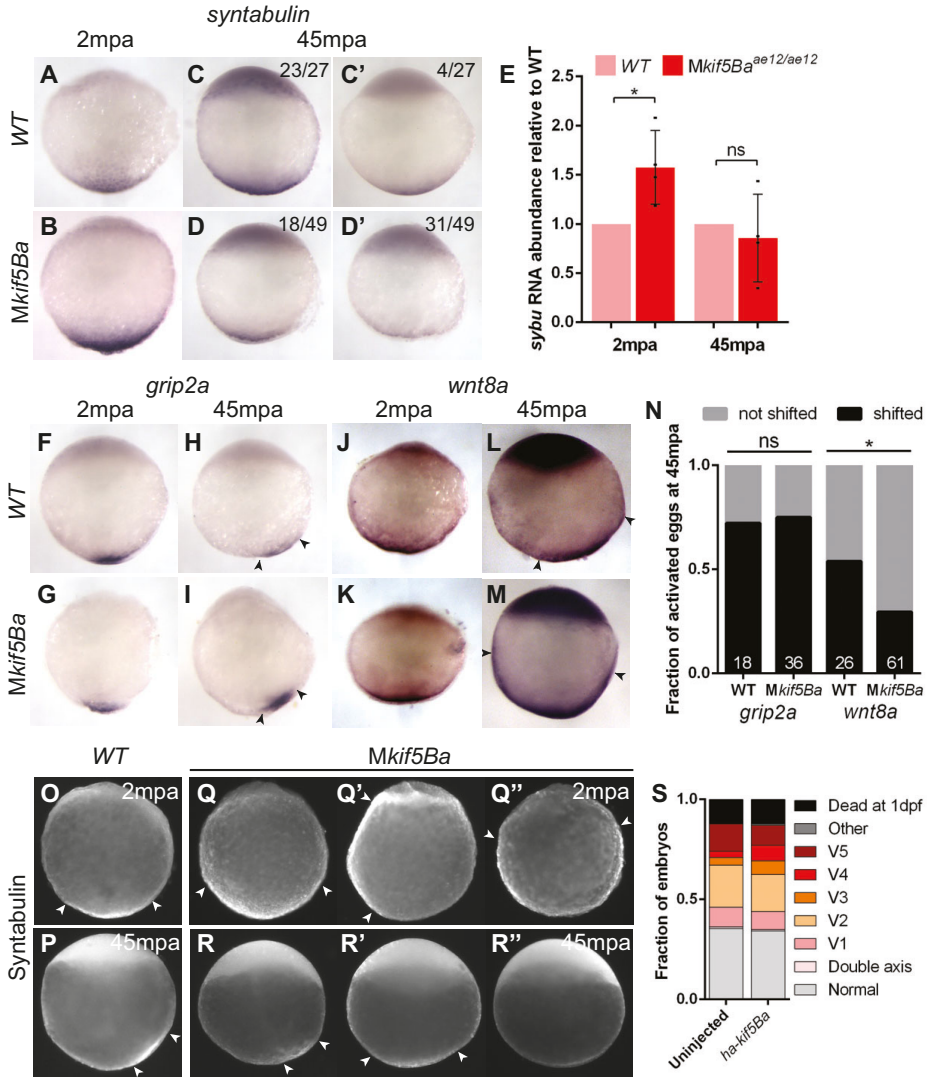

Fig. 6. Maternal *kif5Ba* localizes dorsal determination components in activated eggs. (A-D′) *sybu* is vegetally localized at 2 mpa (A,B) and at 45 mpa (C,D) in both WT (A,C) and M*kif5Ba* mutant (B,D) activated eggs. However, *sybu* is more dispersed at 2 mpa (B) and appears less abundant in most M*kif5Ba* eggs at 45 mpa (D,D′). [2 mpa: *n*=30/30 for M*kif5Ba*$^{ae11/ae12}$ (*N*=2 females), *n*=29/29 for M*kif5Ba*$^{ae12/ae12}$ (*N*=1 female), *n*=63/63 for WT (*N*=3 females) have vegetally localized *sybu*; 45 mpa: quantification in panels.] (E) qRT-PCR reveals significantly more abundant *sybu* RNA in M*kif5Ba* mutants at 2 mpa, although this RNA excess is not maintained at 45 mpa. Error bars show mean±s.d.; Student's *t*-test, **P*=0.0219. (F-I) *grip2a* is vegetally localized at 2 mpa (F,G) and shifts asymmetrically by 45 mpa (H,I) in both WT (F,H) and M*kif5Ba* mutant (G,I) activated eggs. [2 mpa: *n*=37/37 for M*kif5Ba*$^{ae11/ae12}$ (*N*=2 females), *n*=23/23 for WT (*N*=2 females) have vegetally localized *grip2a*; 45 mpa: see N for quantification.] (J-M) *wnt8a* is vegetally localized at 2 mpa in both WT (J) and M*kif5Ba* mutant (K) activated eggs. However, *wnt8a* is asymmetric at 45 mpa in WT (L) but not M*kif5Ba* mutant (M) activated eggs. [2 mpa: *n*=24/24 for M*kif5Ba*$^{ae11/ae12}$ (*N*=2 females), *n*=29/29 for WT (*N*=2 females) have vegetally localized *wnt8a*; 45 mpa: see N for quantification.] (N) Fraction of eggs exhibiting dorsally translocated RNA at 45 mpa. Number at base of columns indicates the number of eggs assayed. Chi-square, *P*=0.0312 (*grip2a*: *n*=2 females for each genotype; *wnt8a: n*=4 M*kif5Ba* and *n*=3 WT females). (O-R″) Sybu is vegetally localized at 2 mpa (O) and is asymmetric at 45 mpa (P) in WT activated eggs. This is normal in some M*kif5Ba* mutant eggs (Q,R), but others show aberrant localization at 2 mpa (Q′,Q″) and at 45 mpa (R′,R″). See text for quantification. (S) Injection of *ha-kif5Ba* RNA into 1-cell-stage M*kif5Ba* mutants fails to suppress DV patterning defects. [*n*=138 uninjected and *n*=81 injected M*kif5Ba*$^{ae11/ae12}$ (*N*=1 female), *n*=172 uninjected and *n*=80 injected M*kif5Ba*$^{ae11/ae12}$ (*N*=2 females)]. Arrowheads designate the lateral limits of each expression domain.

Development (2015) 142, 2996-3008 doi:10.1242/dev.124586

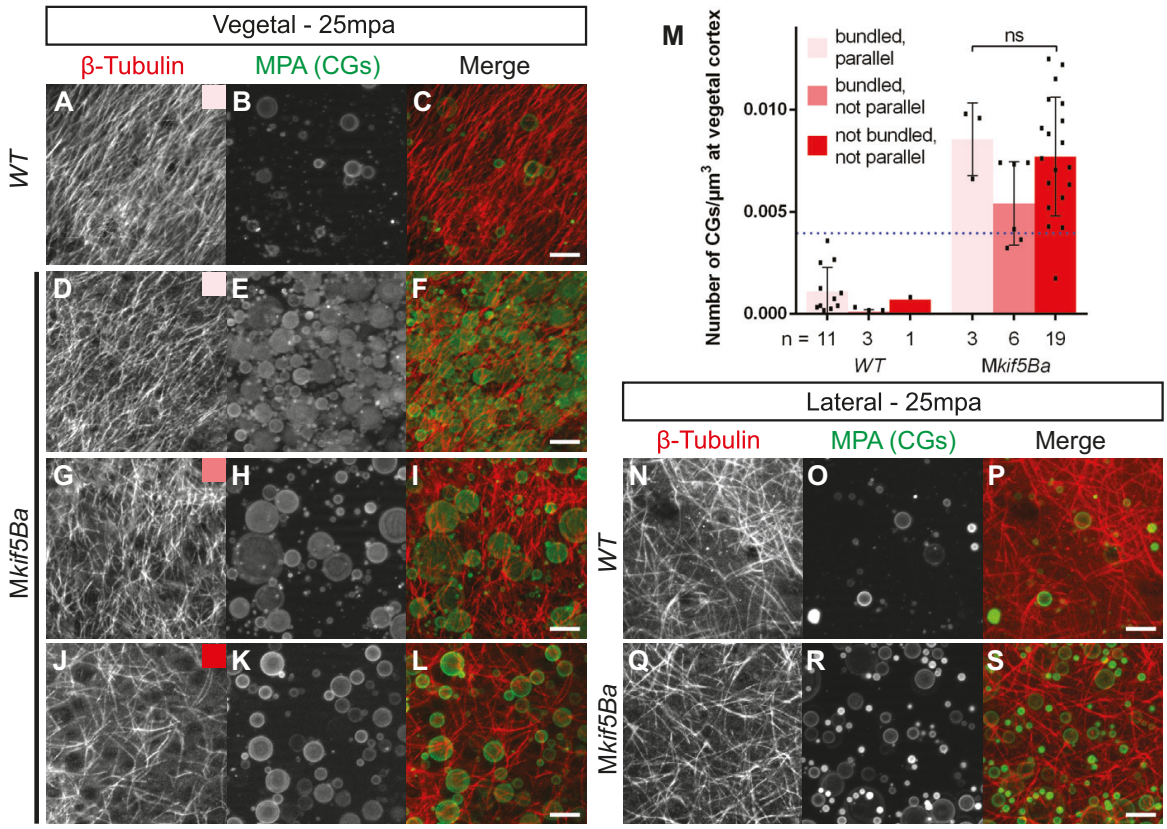

Fig. 7. Maternal *kif5Ba* organizes vegetal microtubules. (A-M) Vegetal microtubules are in a parallel orientation and bundled in WT activated eggs (A), but in M*kif5Ba* mutants are either bundled and parallel (D), bundled but not parallel (G), or not bundled or parallel (J). M*kif5Ba* mutant activated eggs display variable CG exocytosis defects (compare B with E,H,K). Importantly, the degree of CG retention does not correlate with the severity of the microtubule phenotype in M*kif5Ba* mutants (M). Scale bars: 10 µm. Blue dotted line in M represents the upper limit of CG retention observed in WT activated eggs. Error bars show mean±s.d.; one-way ANOVA. (N-S) There is no difference between lateral microtubule organization in WT (N-P) and M*kif5Ba* mutant (Q-S) activated eggs. Scale bars: 10 µm.

Our observation that Buc localization to distal furrows is dynamic, occurring preferentially when chromosomes are decondensed, is consistent with a model whereby Buc seeds GP recruitment and assembly until sufficient GP proteins and RNAs accumulate and Buc is no longer required. Additionally, the distal cleavage furrows are enriched with MTs that form V-shaped structures oriented toward the site of GP assembly during furrow maturation (Jesuthasan, 1998; Urven et al., 2006). Because we observed interactions between Kif5Ba and Buc, it is tempting to speculate that Kif5Ba might mediate transport of Buc to the furrows along these MTs. It is possible that cytoskeletal reorganization accompanying furrow maturation could subsequently account for the dynamic localization of Buc.

Maternal Kif5Ba mediates vegetal microtubule reorganization and the cortical rotation-like event

In zebrafish and *Xenopus*, DV axis specification requires cytoskeletal reorganization to form a pMTA that facilitates asymmetric localization of maternal DDs (Houliston and Elinson, 1991; Jesuthasan and Strähle, 1997). In zebrafish, previous work shows that maternal *grip2a*, *sybu* and *wnt8a* regulate DV patterning (Ge et al., 2014; Lu et al., 2011; Nojima et al., 2010). Grip2a is implicated in pMTA formation, and Syntabulin is hypothesized to tether vegetally localized DDs, such as *wnt8a* (Ge et al., 2014; Lu et al., 2011; Nojima et al., 2010). However, little is known about how these events are regulated.

Our observation that vegetal pMTA formation fails in M*kif5Ba* mutants probably accounts for deficits in *wnt8a* localization and, ultimately, ventralization of mutant progeny. Interestingly, asymmetric localization of *grip2a* is intact in M*kif5Ba* mutants. Previous studies indicate that *grip2a* translocation is disrupted by nocodazole, which disrupts formation of the vegetal pMTA (Ge et al., 2014). Thus, it appears that distinct MT-dependent mechanisms asymmetrically localize cargoes in activated eggs: a Kif5Ba-independent mechanism used by *grip2a*, and a Kif5Ba- and pMTA-dependent mechanism used by *wnt8a* and Sybu. These results raise the interesting possibility that movement of *grip2a* RNA might anticipate vegetal pMTA formation. Interestingly, Grip1, a *grip2a* family member, directly interacts with Kif5s (Setou et al., 2002). Therefore, following *grip2a* RNA translocation, an asymmetric Kif5Ba-Grip2a complex might mediate pMTA formation. Alternatively, Kif5Ba could mediate pMTA formation and bundling by crosslinking MTs using its head and tail MT-binding elements. Such a configuration could also support the zebrafish cortical rotation-like event by MT-MT sliding, as has been described for Kinesin-1 in other contexts (del Castillo et al., 2015; Jolly et al., 2010).

Our finding that *kif5Ba* is required to maintain Sybu at the vegetal cortex and for its subsequent asymmetric translocation supports previous work showing that Sybu interacts with Kif5Ba (Nojima et al., 2010). We also observed that *sybu* RNA was present at higher levels and appeared more dispersed in *Mkif5Ba* mutants following

Development (2015) 142, 2996-3008 doi:10.1242/dev.124586

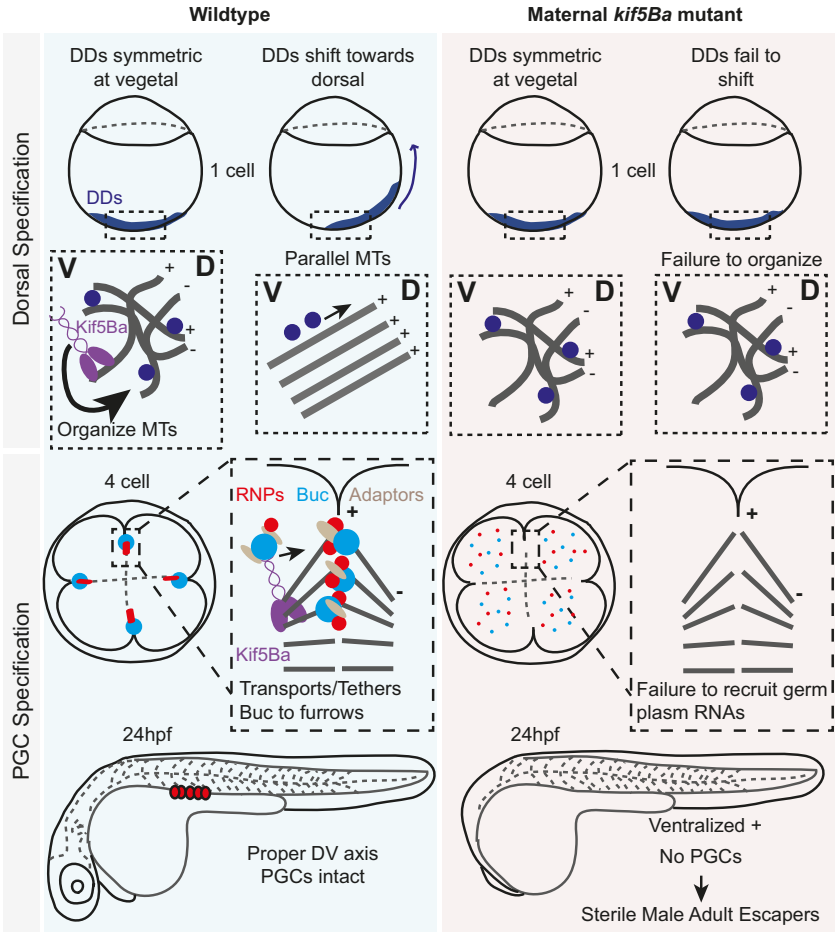

Fig. 8. Model for Kif5Ba functions in dorsoventral patterning and germ cell formation. In WT activated eggs Kif5Ba mediates vegetal pMTA formation and dorsal determinant (DD) translocation towards the prospective dorsal side. Kif5Ba localizes endogenous Buc to distal cleavage furrows and promotes recruitment of GP-RNAs to furrows and subsequent PGC specification. In M*kif5Ba* mutants the vegetal pMTA fails to form, resulting in ventralization. Furthermore, Buc localization to furrows is lost, resulting in failed GP recruitment to specify PGCs and adult sterility. Our data support a model whereby Kif5Ba is required to recruit Buc and GP-RNAs to cleavage furrows, although it is unclear whether it also acts to compact GP-RNAs within distal regions of the cleavage furrow.

egg activation, and that these increased levels were not maintained. Although it is unclear why *sybu* RNA would initially be more abundant, a role for MKif5Ba in tethering *sybu* RNA at the vegetal cortex to protect it from degradation might explain its dispersal and lack of maintenance. Notably, because Sybu was mislocalized at 2 mpa but vegetal localization of *grip2a* and *wnt8a* were intact, this suggests that Sybu probably does not tether these RNAs. It remains possible that Sybu tethers Grip2a or Wnt8a proteins or other uncharacterized DDs. Alternatively, Sybu might contribute to DV patterning by another mechanism.

MATERIALS AND METHODS

Animals

AB strain wild-type zebrafish embryos were obtained from natural pairwise matings and were reared according to standard procedures (Westerfield, 2000). Embryos were raised in 1× Embryo Medium at 28.5°C and staged as described (Kimmel et al., 1995). All procedures and experimental protocols were in accordance with NIH guidelines and approved by the Einstein IACUC (protocol #20140502).

Mutagenesis

kif5Ba zebrafish mutants were created using CRISPR-Cas9-mediated mutagenesis (http://www.addgene.org/crispr/jounglab/CRISPRzebrafish/) (Hwang et al., 2013a,b). A guide RNA (*gRNA*) targeting the motor domain of *kif5Ba* was designed using ZiFiT Targeter software (http://zifit.partners.org/ZiFiT/). The primers *gRNA-F*: TAGGACAGGATAGCGTCGTGAT and *gRNA-R*: AAACATCACGACGCTATCCTGT were annealed and ligated into *Bsa*I-HF-linearized *pDR272* to create *pDR272-kif5Ba-gRNA*. Oligo insertions were sequence-verified, and *gRNAs* were synthesized using MAXIscript T7 Kit (Life Technologies, AM1312M) on *Dra*I-linearized *pDR272-kif5Ba-gRNA*. Cas9 RNA was synthesized using mMESSAGE mMACHINE SP6 Transcription Kit (Life Technologies, AM1340) on *Mss*I-linearized MLM3613 and poly-Adenylated with the Poly(A) Tailing Kit (Life Technologies, AM1350). *gRNA* and Cas9 RNA were co-injected (2 nl at 12.5 ng/µl and 300 ng/µl, respectively). T7 endonuclease I assays (Hwang et al., 2013b) and sequencing were used to determine mutagenesis efficiency. Injected embryos were raised to adulthood, their progeny were screened, and two founders bearing distinct mutations were identified and propagated.

Genotyping

Genomic DNA was extracted from adult fins or embryos using standard procedures (Westerfield, 2000). The region surrounding the *kif5Ba*^{ae11} and *kif5Ba*^{ae12} mutations was amplified with primers 5′-GGAGTGCACCATTAAAGTCATGTG and 5′-GTCGGTGTCAAATATTGAGGTC. Restriction enzyme (RE) digestion with *Pvu*I for *kif5Ba*^{ae11} produced two smaller fragments for the mutant allele. RE digestion with *Mbo*I for *kif5Ba*^{ae12} produced two smaller fragments for the wild-type allele but not the mutant allele.

In situ hybridization

For chromogenic *in situ* hybridization, embryos or activated eggs at the specified stages were fixed in 4% paraformaldehyde overnight at 4°C. *In situ* hybridization was performed according to Thisse and Thisse (2014), except that maleic acid buffer (100 mM maleic acid, pH 8, 150 mM NaCl) was substituted for PBS during antibody incubations and BM Purple was used to develop (Roche, 1442074). FISHs were performed using the Multiplex Fluorescent Reagent Kit (ACD Bio, 320850) according to the whole-mount RNAscope protocol (Gross-Thebing et al., 2014). Dissected ovaries were fixed for 30 min in 4% paraformaldehyde at room temperature (RT), washed with PBT (0.1% Tween), dehydrated in MeOH and placed at −20°C

Development (2015) 142, 2996-3008 doi:10.1242/dev.124586

overnight. RNAscope *Blank C1 probe*, *Dr-nanos3-C2 probe* (ACD Bio, 404521-C2) and *Dr-vasa-C3 probe* (ACD Bio, 407271-C3) were used.

Immunofluorescence and F-actin, cortical granule and DiOC6 labeling

For whole-mount IF of microtubules, F-actin and Buc, eggs and embryos were fixed with microtubule staining buffer (80 mM K-PIPES pH 6.8, 5 mM EGTA, 1 mM $MgCl_2$, 3.7% formaldehyde, 0.25% glutaraldehyde, 0.2% Triton X-100) for 4-5 h at RT. Staining was performed immediately. All other stainings: embryos or ovaries were fixed in 4% paraformaldehyde overnight at 4°C, dehydrated in MeOH and placed at −20°C. Anti-β-tubulin (Millipore, MAB3408) was diluted at 1:1000, Anti-Bucky ball y1165 at 1:500 (Heim et al., 2014), Anti-Syntabulin Syn1 at 1:1000 (Nojima et al., 2010), Anti-Vasa at 1:5000 (Knaut et al., 2000) and Anti-HA at 1:500 (Roche, 11867423001). Alexa Fluor 488 and Alexa Fluor 568 (Molecular Probes) secondary antibodies were diluted at 1:500. CGs were stained by incubation in 50 µg/ml FITC-conjugated *Maclura pomifera* lectin (EY Labs, F-3901-2) for 90 min at RT in PBS-Triton X-100. CGs were counted in a defined vegetal region at depth×height×width of 4 µm×59.45 µm×59.45 µm. F-actin was stained by incubating with Rhodamine-Phalloidin (Life Technologies, R415) at 1:50 overnight at 4°C. DiOC6 staining was performed as previously described (Marlow and Mullins, 2008).

RT-PCR

Total RNA was extracted from pooled embryos (n=20-30/stage) using Trizol (Life Technologies, 15596). cDNA was prepared with SuperScript III Reverse Transcription Kit (Life Technologies, 18080-051). RT-PCR was performed using the following primers: *ef1α* (Fig. 1) and *vasa*: (Heim et al., 2014); *dazl* and *nanos3* (Hartung et al., 2014); *kif5Ba*: 5′-GACTTTGCACAACCTCAGGAAA and 5′-GCAGACGCTTCTCCAGTTTAGG; *ef1α* (Fig. 6): 5′-CTGGTTCAAGGGATGGAAGA and 5′-CTGGTTCAAGGGATGGAAGA; *sybu*: 5′-GGAAGCTACAAGACCCGAGAAA and 5′-TGATGCCATGATTGTCTCCACA. qRT-PCR reactions were performed in triplicate with SYBR Green Master Mix (Thermo Scientific) and an Eppendorf realplex^2 Mastercycler. Expression relative to WT was quantified with the ΔΔCt method using *ef1α* as the standard gene.

Histology

Females or males were anesthetized in Tricaine as described (Westerfield, 2000), and the ovaries or testes were dissected and fixed in 4% paraformaldehyde overnight at 4°C. Fixed ovaries were washed in PBS, dehydrated in methanol, embedded in paraffin and sectioned. Deparaffinized slides were stained in H&E, coated with Permount solution (Fisher Scientific), coverslipped and imaged. Oocytes were staged according to Selman et al. (1993).

RNA injection

ha-kif5Ba RNA was transcribed from *pCS2+HA-Kif5Ba* (Nojima et al., 2010) with the mMESSAGE mMACHINE SP6 Transcription Kit (Life Technologies, AM1340). *pCS-GFP-Buc* was created by recombining *pCR8-cbuc80* (Heim et al., 2014) with *pCSGFPDest* (Villefranc et al., 2007) (Invitrogen). *gfp-buc* RNA was transcribed from *pCS-GFP-Buc* with the mMESSAGE mMACHINE SP6 Transcription Kit. *cherry-24xMBS* RNA was used as a control and prepared as previously described (Campbell et al., 2015). Embryos from *kif5Ba*$^{-/-}$ females were collected within 15 min of spawning. Approximately 1 nl of 500-800 ng/µl (*ha-kif5Ba* or *cherry-MBS*) or 400 ng/µl (*gfp-buc*) injection solution was injected into 1-cell-stage embryos.

Buc pull-down

To reduce yolk content, ovaries were dissected from *alk6b*$^{-/-}$ adults (Neumann et al., 2011) and lysed in RIPA buffer. To pre-clear the lysate and to bind the antibody, respectively, 500 µg ovary lysate+50 µl Protein G beads (New England Biolabs, S1430S) and 50 µl Protein-G beads+100 µl y1165 (Heim et al., 2014) were simultaneously incubated at 4°C for 1 h. Pre-cleared lysate and antibody-bound beads were incubated at 4°C for 1 h and beads were then washed with RIPA. Proteins were eluted in 60 µl SDS-BME at 70°C for 5 min. Eluates were run on pre-cast polyacrylamide gels (Bio-Rad, 161-1174), stained with Gel Code Blue stain (Pierce, PI24592), and bands were extracted and analyzed with mass spectrometry and Scaffold software (Einstein Proteomics Facility).

Co-immunoprecipitation in HEK293T cells

HEK293T cells were transfected with *pCS-GFP-Buc* and *pCS2+HA-Kif5Ba* (Nojima et al., 2010) using Optimem (Life Technologies, 31985) and PEI, and lysed at 48 h post-transfection using RIPA plus protease-inhibitors (Sigma, P2714). Lysates were pre-cleared with Protein-G Beads (New England Biolabs, S1430S) at 4°C for 1 h, then immunoprecipitated with anti-GFP antibody clone 3E6 (Life Technologies, A11120). Eluates were run on Fisher EZ-Run 12.5% SDS-PAGE (Fisher, BP7712) and blotted with anti-HA 3F10 antibody (Roche, 11867423001). Proteins were detected with HRP-conjugated anti-Rat IgG (H+L) (Jackson ImmunoResearch, 112-036-003), using the Amersham ECL Plus Chemiluminescence kit (GE Healthcare, RPN2132).

Image acquisition and processing

Whole-mount chromogenic *in situ* hybridization and live whole-mount 1 dpf embryos were imaged using an Olympus SZ61 dissecting microscope with a high-resolution digital camera (model S97809, Olympus America) and Picture Frame 3.0 software (Optronics). H&E stainings were imaged using a Zeiss Axioskop2 plus microscope with a Zeiss AxioCam MRc camera and Zeiss AxioVision Rel. 4.6 software. Anti-Syntabulin-stained eggs, RNAscope *in situ* hybridization, cytoskeleton at the cleavage furrows, oocyte immunofluorescence and anti-Vasa-stained embryos were imaged using a Zeiss Axio Observer inverted microscope equipped with Apotome and AxioCam MRm CCD camera and Zeiss AxioVision Rel. 4.6 software. Vegetal microtubules and high magnification anti-Vasa-stained PGCs were imaged using a Zeiss 5Live Duoscan line-scanning confocal microscope.

Acknowledgements

We thank F. Pelegri, M. Hibi and H. Knaut for reagents, Marlow lab members for discussions, our animal staff, and the Analytical Imaging (NCI P30CA013330), Histotechnology and Proteomics Facilities for technical support.

Competing interests

The authors declare no competing or financial interests.

Author contributions

P.D.C. and M.Z.S. identified *kif5Ba* alleles. P.D.C., A.E.H. and F.L.M. performed dissections and histological analysis. P.D.C. and A.E.H. performed all other experiments and analysis in consultation with F.L.M. P.D.C., A.E.H. and F.L.M. conceived and designed experiments. F.L.M. contributed reagents, materials and analysis tools. All authors discussed data and the manuscript. P.D.C. and F.L.M. wrote the manuscript.

Funding

This work was supported by the National Institutes of Health [R01GM089979 and start-up funds to F.L.M.; T32-GM007288 and 1F31NS083258 to P.D.C.]. Deposited in PMC for release after 12 months.

Supplementary material

Supplementary material available online at
http://dev.biologists.org/lookup/suppl/doi:10.1242/dev.124586/-/DC1

References

Becker, K. A. and Hart, N. H. (1996). The cortical actin cytoskeleton of unactivated zebrafish eggs: spatial organization and distribution of filamentous actin, nonfilamentous actin, and myosin-II. *Mol. Reprod. Dev.* **43**, 536-547.

Becker, K. A. and Hart, N. H. (1999). Reorganization of filamentous actin and myosin-II in zebrafish eggs correlates temporally and spatially with cortical granule exocytosis. *J. Cell Sci.* **112**, 97-110.

Bontems, F., Stein, A., Marlow, F., Lyautey, J., Gupta, T., Mullins, M. C. and Dosch, R. (2009). Bucky ball organizes germ plasm assembly in zebrafish. *Curr. Biol.* **19**, 414-422.

Braat, A. K., Zandbergen, T., Van de Water, S., Goos, H. J. T. and Zivkovic, D. (1999). Characterization of zebrafish primordial germ cells: morphology and early distribution of vasa RNA. *Dev. Dyn.* **216**, 153-167.

Cai, Q., Gerwin, C. and Sheng, Z.-H. (2005). Syntabulin-mediated anterograde transport of mitochondria along neuronal processes. *J. Cell Biol.* **170**, 959-969.
Campbell, P. D. and Marlow, F. L. (2013). Temporal and tissue specific gene expression patterns of the zebrafish kinesin-1 heavy chain family, kif5s, during development. *Gene Expr. Patterns* **13**, 271-279.
Campbell, P. D., Chao, J. A., Singer, R. H. and Marlow, F. L. (2015). Dynamic visualization of transcription and RNA subcellular localization in zebrafish. *Development* **142**, 1368-1374.
Chang, N., Sun, C., Gao, L., Zhu, D., Xu, X., Zhu, X., Xiong, J.-W. and Xi, J. J. (2013). Genome editing with RNA-guided Cas9 nuclease in zebrafish embryos. *Cell Res.* **23**, 465-472.
del Castillo, U., Lu, W., Winding, M., Lakonishok, M. and Gelfand, V. I. (2015). Pavarotti/MKLP1 regulates microtubule sliding and neurite outgrowth in drosophila neurons. *Curr. Biol.* **25**, 200-205.
Dosch, R. (2014). Next generation mothers: maternal control of germline development in zebrafish. *Crit. Rev. Biochem. Mol. Biol.* **50**, 54-68.
Dosch, R., Wagner, D. S., Mintzer, K. A., Runke, G., Wiemelt, A. P. and Mullins, M. C. (2004). Maternal control of vertebrate development before the midblastula transition: mutants from the zebrafish I. *Dev. Cell* **6**, 771-780.
Draper, B. W., McCallum, C. M. and Moens, C. B. (2007). nanos1 is required to maintain oocyte production in adult zebrafish. *Dev. Biol.* **305**, 589-598.
Eno, C. and Pelegri, F. (2013). Gradual recruitment and selective clearing generate germ plasm aggregates in the zebrafish embryo. *Bioarchitecture* **3**, 125-132.
Ewen-Campen, B., Schwager, E. E. and Extavour, C. G. M. (2010). The molecular machinery of germ line specification. *Mol. Reprod. Dev.* **77**, 3-18.
Gagnon, J. A., Kreiling, J. A., Powrie, E. A., Wood, T. R. and Mowry, K. L. (2013). Directional transport is mediated by a Dynein-dependent step in an RNA localization pathway. *PLoS Biol.* **11**, e1001551.
Ge, X., Grotjahn, D., Welch, E., Lyman-Gingerich, J., Holguin, C., Dimitrova, E., Abrams, E. W., Gupta, T., Marlow, F. L., Yabe, T. et al. (2014). Hecate/Grip2a acts to reorganize the cytoskeleton in the symmetry-breaking event of embryonic axis induction. *PLoS Genet.* **10**, e1004422.
Gerhart, J., Danilchik, M., Doniach, T., Roberts, S., Rowning, B. and Stewart, R. (1989). Cortical rotation of the Xenopus egg: consequences for the anteroposterior pattern of embryonic dorsal development. *Development* **107** Suppl., 37-51.
Gross-Thebing, T., Paksa, A. and Raz, E. (2014). Simultaneous high-resolution detection of multiple transcripts combined with localization of proteins in whole-mount embryos. *BMC Biol.* **12**, 55.
Hartung, O. M. and Marlow, F. L. (2014). Get it together: how RNA-binding proteins assemble and regulate germ plasm in the oocyte and embryo. In *Zebrafish: Topics in Reproduction, Toxicology and Development* (ed. C. A. Lessman and E. A. Carver), pp. 65-106. Hauppauge, NY, USA: Nova Science Publishers.
Hartung, O., Forbes, M. M. and Marlow, F. L. (2014). Zebrafish vasa is required for germ-cell differentiation and maintenance. *Mol. Reprod. Dev.* **81**, 946-961.
Hashimoto, Y., Maegawa, S., Nagai, T., Yamaha, E., Suzuki, H., Yasuda, K. and Inoue, K. (2004). Localized maternal factors are required for zebrafish germ cell formation. *Dev. Biol.* **268**, 152-161.
Hathaway, D. S. and Selman, G. G. (1961). Certain aspects of cell lineage and morphogenesis studied in embryos of Drosophila melanogaster with an ultra-violet micro-beam. *J. Embryol. Exp. Morphol.* **9**, 310-325.
Heim, A. E., Hartung, O., Rothhamel, S., Ferreira, E., Jenny, A. and Marlow, F. L. (2014). Oocyte polarity requires a Bucky ball-dependent feedback amplification loop. *Development* **141**, 842-854.
Houliston, E. and Elinson, R. P. (1991). Evidence for the involvement of microtubules, ER, and kinesin in the cortical rotation of fertilized frog eggs. *J. Cell Biol.* **114**, 1017-1028.
Howley, C. and Ho, R. K. (2000). mRNA localization patterns in zebrafish oocytes. *Mech. Dev.* **92**, 305-309.
Hruscha, A., Krawitz, P., Rechenberg, A., Heinrich, V., Hecht, J., Haass, C. and Schmid, B. (2013). Efficient CRISPR/Cas9 genome editing with low off-target effects in zebrafish. *Development* **140**, 4982-4987.
Hwang, W. Y., Fu, Y., Reyon, D., Maeder, M. L., Kaini, P., Sander, J. D., Joung, J. K., Peterson, R. T. and Yeh, J.-R. (2013a). Heritable and precise zebrafish genome editing using a CRISPR-Cas system. *PLoS ONE* **8**, e68708.
Hwang, W. Y., Fu, Y., Reyon, D., Maeder, M. L., Tsai, S. Q., Sander, J. D., Peterson, R. T., Yeh, J.-R. J. and Joung, J. K. (2013b). Efficient genome editing in zebrafish using a CRISPR-Cas system. *Nat. Biotechnol.* **31**, 227-229.
Illmensee, K. and Mahowald, A. P. (1974). Transplantation of posterior polar plasm in Drosophila. Induction of germ cells at the anterior pole of the egg. *Proc. Natl. Acad. Sci. USA* **71**, 1016-1020.
Jesuthasan, S. (1998). Furrow-associated microtubule arrays are required for the cohesion of zebrafish blastomeres following cytokinesis. *J. Cell Sci.* **111**, 3695-3703.
Jesuthasan, S. and Strähle, U. (1997). Dynamic microtubules and specification of the zebrafish embryonic axis. *Curr. Biol.* **7**, 31-42.
Jolly, A. L., Kim, H., Srinivasan, D., Lakonishok, M., Larson, A. G. and Gelfand, V. I. (2010). Kinesin-1 heavy chain mediates microtubule sliding to drive changes in cell shape. *Proc. Natl. Acad. Sci. USA* **107**, 12151-12156.
Kimmel, C. B., Ballard, W. W., Kimmel, S. R., Ullmann, B. and Schilling, T. F. (1995). Stages of embryonic development of the zebrafish. *Dev. Dyn.* **203**, 253-310.
Kloc, M., Bilinski, S. and Etkin, L. D. (2004). The Balbiani body and germ cell determinants: 150 years later. *Curr. Top. Dev. Biol.* **59**, 1-36.
Knaut, H., Pelegri, F., Bohmann, K., Schwarz, H. and Nüsslein-Volhard, C. (2000). Zebrafish vasa RNA but not its protein is a component of the germ plasm and segregates asymmetrically before germline specification. *J. Cell Biol.* **149**, 875-888.
Koprunner, M., Thisse, C., Thisse, B. and Raz, E. (2001). A zebrafish nanos-related gene is essential for the development of primordial germ cells. *Genes Dev.* **15**, 2877-2885.
Kosaka, K., Kawakami, K., Sakamoto, H. and Inoue, K. (2007). Spatiotemporal localization of germ plasm RNAs during zebrafish oogenesis. *Mech. Dev.* **124**, 279-289.
Langdon, Y. G. and Mullins, M. C. (2011). Maternal and zygotic control of zebrafish dorsoventral axial patterning. *Annu. Rev. Genet.* **45**, 357-377.
Lesch, B. J. and Page, D. C. (2012). Genetics of germ cell development. *Nat. Rev. Genet.* **13**, 781-794.
Lu, F.-I., Thisse, C. and Thisse, B. (2011). Identification and mechanism of regulation of the zebrafish dorsal determinant. *Proc. Natl. Acad. Sci. USA* **108**, 15876-15880.
Maegawa, S., Yasuda, K. and Inoue, K. (1999). Maternal mRNA localization of zebrafish DAZ-like gene. *Mech. Dev.* **81**, 223-226.
Marlow, F. L. (2010). *Maternal Control of Development in Vertebrates: My Mother Made Me Do It!* San Rafael, CA, USA: Morgan & Claypool Life Sciences.
Marlow, F. L. and Mullins, M. C. (2008). Bucky ball functions in Balbiani body assembly and animal-vegetal polarity in the oocyte and follicle cell layer in zebrafish. *Dev. Biol.* **321**, 40-50.
Marrari, Y., Terasaki, M., Arrowsmith, V. and Houliston, E. (2000). Local inhibition of cortical rotation in Xenopus eggs by an anti-KRP antibody. *Dev. Biol.* **224**, 250-262.
Mei, W., Lee, K. W., Marlow, F. L., Miller, A. L. and Mullins, M. C. (2009). hnRNP I is required to generate the Ca2+ signal that causes egg activation in zebrafish. *Development* **136**, 3007-3017.
Messitt, T. J., Gagnon, J. A., Kreiling, J. A., Pratt, C. A., Yoon, Y. J. and Mowry, K. L. (2008). Multiple kinesin motors coordinate cytoplasmic RNA transport on a subpopulation of microtubules in Xenopus oocytes. *Dev. Cell* **15**, 426-436.
Nair, S., Marlow, F., Abrams, E., Kapp, L., Mullins, M. C. and Pelegri, F. (2013). The chromosomal passenger protein birc5b organizes microfilaments and germ plasm in the zebrafish embryo. *PLoS Genet.* **9**, e1003448.
Neumann, J. C., Chandler, G. L., Damoulis, V. A., Fustino, N. J., Lillard, K., Looijenga, L., Margraf, L., Rakheja, D. and Amatruda, J. F. (2011). Mutation in the type IB bone morphogenetic protein receptor Alk6b impairs germ-cell differentiation and causes germ-cell tumors in zebrafish. *Proc. Natl. Acad. Sci. USA* **108**, 13153-13158.
Nijjar, S. and Woodland, H. R. (2013). Protein interactions in Xenopus germ plasm RNP particles. *PLoS ONE* **8**, e80077.
Nojima, H., Rothhamel, S., Shimizu, T., Kim, C.-H., Yonemura, S., Marlow, F. L. and Hibi, M. (2010). Syntabulin, a motor protein linker, controls dorsal determination. *Development* **137**, 923-933.
Pelegri, F., Knaut, H., Maischein, H.-M., Schulte-Merker, S. and Nüsslein-Volhard, C. (1999). A mutation in the zebrafish maternal-effect gene nebel affects furrow formation and vasa RNA localization. *Curr. Biol.* **9**, 1431-1440.
Raz, E. and Reichman-Fried, M. (2006). Attraction rules: germ cell migration in zebrafish. *Curr. Opin. Genet. Dev.* **16**, 355-359.
Schneider, S., Steinbeisser, H., Warga, R. M. and Hausen, P. (1996). Beta-catenin translocation into nuclei demarcates the dorsalizing centers in frog and fish embryos. *Mech. Dev.* **57**, 191-198.
Seervai, R. N. H. and Wessel, G. M. (2013). Lessons for inductive germline determination. *Mol. Reprod. Dev.* **80**, 590-609.
Selman, K., Wallace, R. A., Sarka, A. and Qi, X. (1993). Stages of oocyte development in the zebrafish, Brachydanio rerio. *J. Morphol.* **218**, 203-224.
Setou, M., Seog, D.-H., Tanaka, Y., Kanai, Y., Takei, Y., Kawagishi, M. and Hirokawa, N. (2002). Glutamate-receptor-interacting protein GRIP1 directly steers kinesin to dendrites. *Nature* **417**, 83-87.
Su, Q., Cai, Q., Gerwin, C., Smith, C. L. and Sheng, Z.-H. (2004). Syntabulin is a microtubule-associated protein implicated in syntaxin transport in neurons. *Nat. Cell Biol.* **6**, 941-953.
Theusch, E. V., Brown, K. J. and Pelegri, F. (2006). Separate pathways of RNA recruitment lead to the compartmentalization of the zebrafish germ plasm. *Dev. Biol.* **292**, 129-141.
Thisse, B. and Thisse, C. (2014). In situ hybridization on whole-mount zebrafish embryos and young larvae. *Methods Mol. Biol.* **1211**, 53-67.
Togashi, S., Kobayashi, S. and Okada, M. (1986). Functions of maternal mRNA as a cytoplasmic factor responsible for pole cell formation in Drosophila embryos. *Dev. Biol.* **118**, 352-360.

Development (2015) 142, 2996-3008 doi:10.1242/dev.124586

Tran, L. D., Hino, H., Quach, H., Lim, S., Shindo, A., Mimori-Kiyosue, Y., Mione, M., Ueno, N., Winkler, C., Hibi, M. et al. (2012). Dynamic microtubules at the vegetal cortex predict the embryonic axis in zebrafish. *Development* **139**, 3644-3652.

Urven, L. E., Yabe, T. and Pelegri, F. (2006). A role for non-muscle myosin II function in furrow maturation in the early zebrafish embryo. *J. Cell Sci.* **119**, 4342-4352.

Villefranc, J. A., Amigo, J. and Lawson, N. D. (2007). Gateway compatible vectors for analysis of gene function in the zebrafish. *Dev. Dyn.* **236**, 3077-3087.

Westerfield, M. (2000). *The Zebrafish Book. A Guide for the Laboratory Use of Zebrafish (Danio rerio)*, 4th edn. Eugene: University of Oregon Press.

Yabe, T., Ge, X., Lindeman, R., Nair, S., Runke, G., Mullins, M. C. and Pelegri, F. (2009). The maternal-effect gene cellular island encodes aurora B kinase and is essential for furrow formation in the early zebrafish embryo. *PLoS Genet.* **5**, e1000518.

Yoon, C., Kawakami, K. and Hopkins, N. (1997). Zebrafish vasa homologue RNA is localized to the cleavage planes of 2- and 4-cell-stage embryos and is expressed in the primordial germ cells. *Development* **124**, 3157-3165.

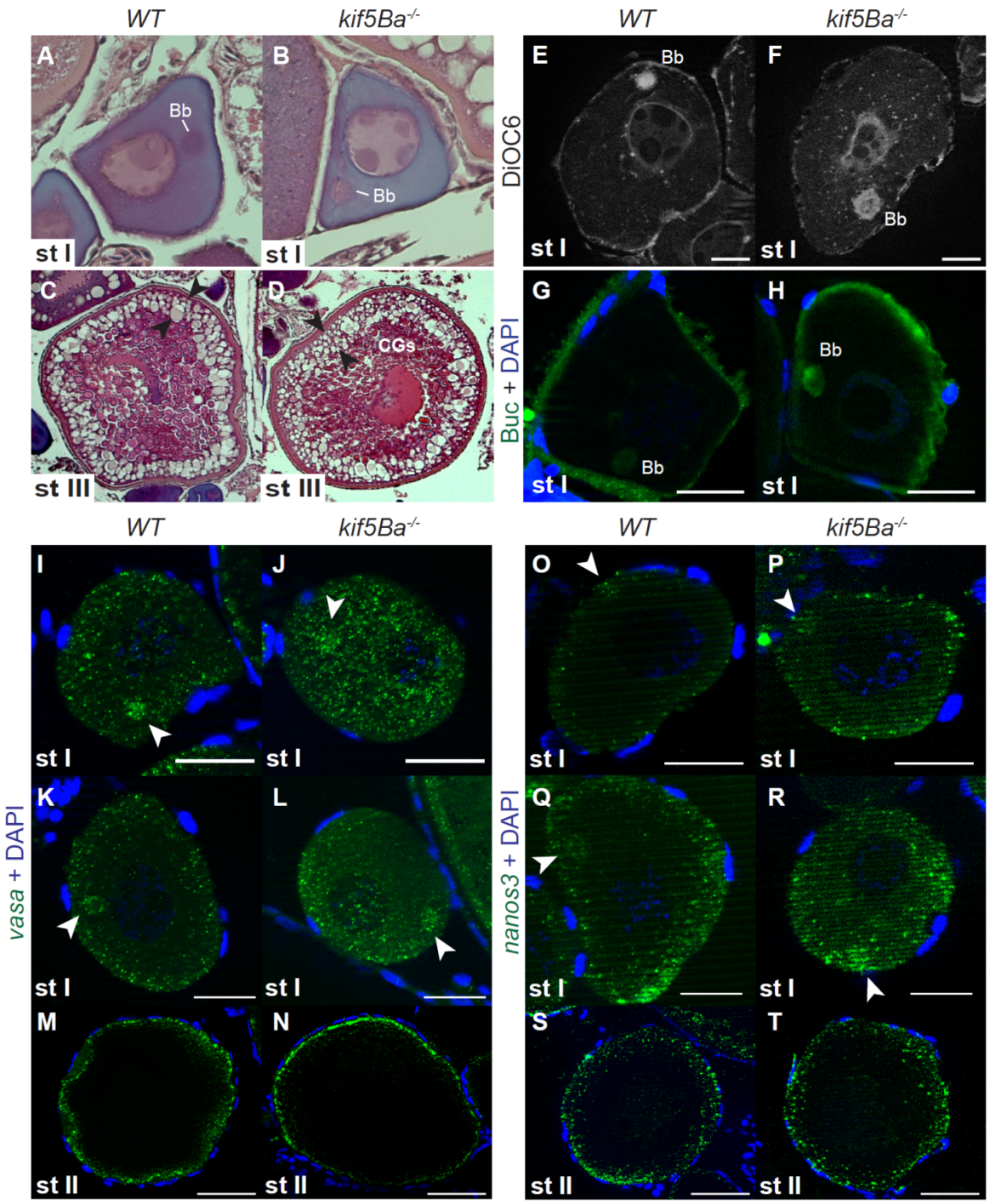

Figure S1. *kif5Ba* is dispensable for oocyte polarity and germ plasm localization.

(A-D) H&E staining of WT (A,C) and *kif5Ba*$^{-/-}$ mutant (B,D) oocytes showing polarized stage I (st I) oocytes with Balbiani bodies (Bb) and normal stage III (st III) oocytes with cortically-localized cortical granules (CGs, between arrowheads) and centrally localized

nucleus and yolk. (n=3 mutant ovaries analyzed, one each of *kif5Ba*$^{ae11/ae11}$, *kif5Ba*$^{ae11/ae12}$, and *kif5Ba*$^{ae12/ae12}$; assayed 5-10 oocytes for each genotype).

(E-F) DiOC6 staining reveals that ER and mitochondria are properly localized to the Bb in WT (E) and *kif5Ba*$^{-/-}$ mutant (F) st I oocytes. (n=18 oocytes analyzed from *kif5Ba*$^{ae11/ae11}$ mutant ovary, n=19 oocytes analyzed from WT ovary). Scale bars 20μm.

(G-H) Buc is properly localized to the Bb in WT (G) and *kif5Ba*$^{-/-}$ mutant (H) st I oocytes. (n=12 oocytes analyzed from *kif5Ba*$^{ae11/ae11}$ mutant ovary, n=10 oocytes analyzed from WT ovary)). Scale bars 20μm.

(I-T) *vasa* (I-N) and *nanos3* (O-T) RNA are enriched in the Bb (arrowheads) in early st I (I,J,O,P) and late st I (K,L,Q,R) oocytes in WT (I,K,O,Q) and *kif5Ba*$^{-/-}$ mutants (J,L,P,R). *vasa* RNA localizes to the cortex in WT (M) and *kif5Ba*$^{-/-}$ mutant (N) st II oocytes. *nanos3* RNA is diffuse throughout the cytosol of WT (S) and *kif5Ba*$^{-/-}$ mutant (T) st II oocytes. (n=3 WT and *kif5Ba*$^{ae12/ae12}$ mutant ovaries, assayed ≥10 oocytes for each condition). Scale bars 25μm (I-L, O-R), 25μm (M,N,S,T).

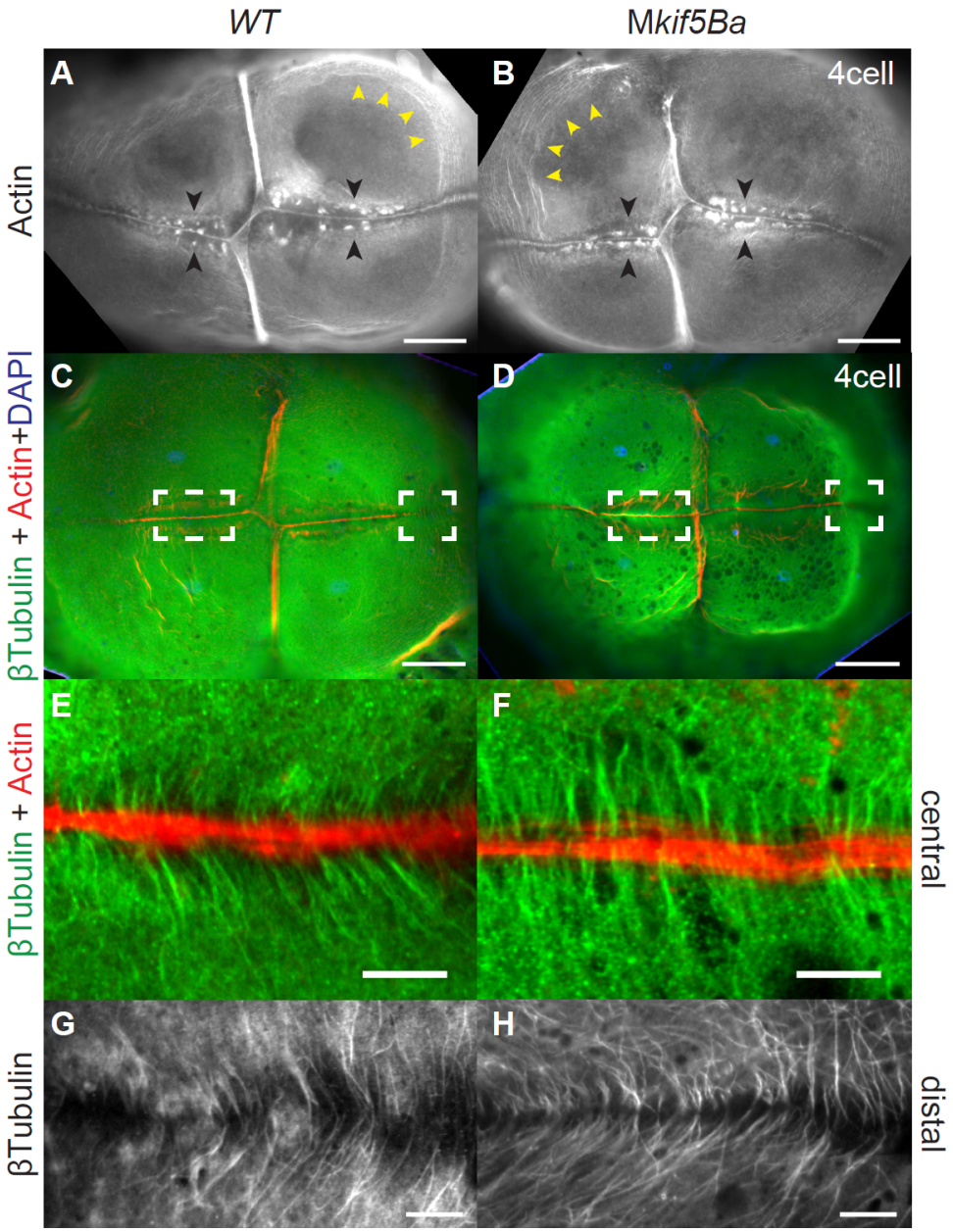

Figure S2. Cleavage furrow-associated cytoskeleton is intact in M*kif5Ba* mutants.

(A-B) Rhodamine-phalloidin staining to label F-actin. Animal pole views reveal an F-actin contractile band present in all four furrows, F-actin accumulations flanking the FMA (black arrowheads) and circumferential actin bands around the blastomeres (yellow arrowheads) in both WT (A) and Mkif5Ba mutants (B). Scale bars, 100μm.

(C-D) β-Tubulin antibody staining to reveal microtubules. Animal pole views show the F-actin contractile band present in all four furrows and the furrow microtubule arrays that flank the newly forming furrows of WT (C) and M*kif5Ba* mutants (D). Left and right dotted boxes in each panel indicate central and distal regions of the newly forming furrow respectively. Scale bars, 100μm.

(E-F) Higher magnification of the central furrow shows that the furrow microtubules are parallel to each other and perpendicular to the F-actin contractile band in both WT (E) and M*kif5Ba* mutants (F). Scale bars, 10μm.

(G-H) Higher magnification of the distal furrow shows microtubules angled in a V-shaped configuration pointing towards the distal end in both WT (G) and M*kif5Ba* mutants (H). Scale bars, 10μm. (All results are from n=11 embryos for M$kif5Ba^{ae11/ae12}$, n=9 for M$kif5Ba^{ae11/ae11}$, and n=15 for WT).

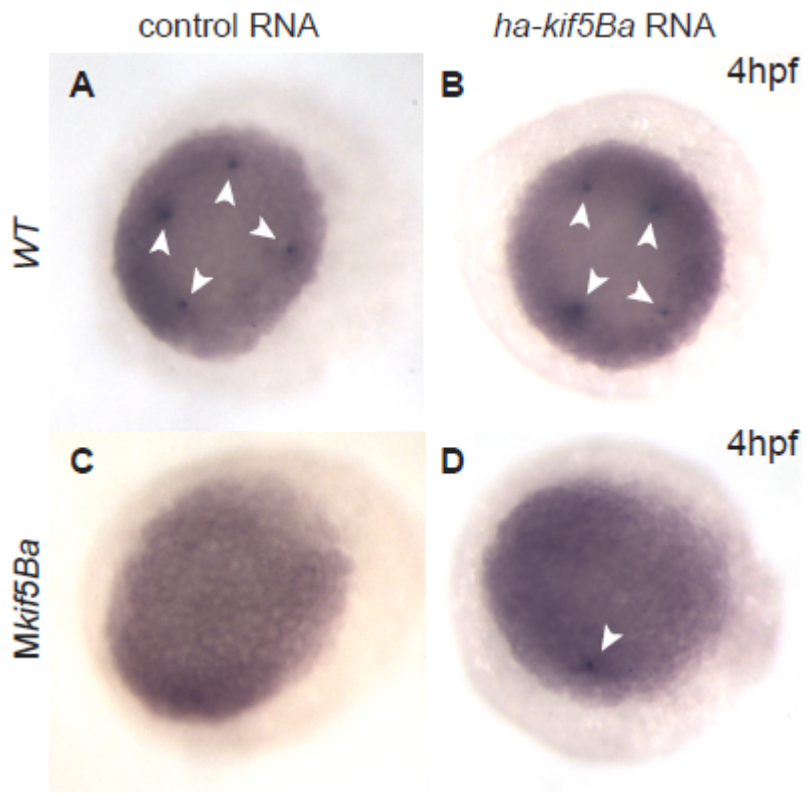

Figure S3. Injection of control RNA has no effect on number of PGCs in WT or M*kif5Ba* mutant embryos.

(A-B) The is no difference in the number of *nanos3*-positive PGCs at 4hpf in embryos injected with either 800pg of a control RNA encoding Cherry protein (A; 3.46±0.26 PGCs in n=37 embryos) or 800pg of *ha-kif5Ba* RNA (B; 3.56±0.25 PGCs in n=32 embryos)

(C-D) While injection of 800pg of a control RNA encoding Cherry protein has no effect on the number of PGCs in M*kif5Ba* mutants (C; zero PGCs in n=42/43 embryos, one PGC in n=1/43 embryos) injection of 800pg of *ha-kif5Ba* leads to the appearance of one PGC in a subset of M*kif5Ba* mutants (D; one PGC visible in 13/85 embryos). Compare with uninjected M*kif5Ba* mutants (zero PGCs in n=72/73 embryos, one PGC in n=1/73 embryos).

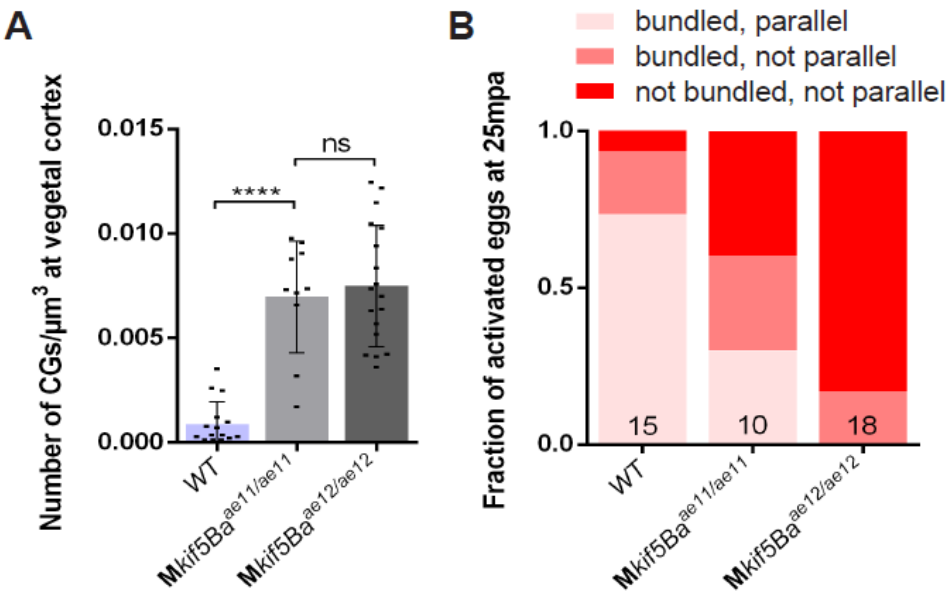

Figure S4. Severity of vegetal microtubule defect correlates with genotype and not degree of CG retention.

(A) There is no difference between the density of retained CGs at vegetal cortex at 25mpa in M*kif5Ba*$^{ae11/ae11}$ and M*kif5Ba*$^{ae12/ae12}$ mutants. Mean ± SD. One-way ANOVA, **** p<0.0001.

(B) The vegetal microtubules are more disorganized in M*kif5Ba*$^{ae12/ae12}$ compared to M*kif5Ba*$^{ae11/ae11}$ mutants.